Digital Comprehensive Summaries of Uppsala Dissertations
from the Faculty of Science and Technology 2311

Analytic Element Models for Groundwater Flow and Linear Elasticity in Fractured Rocks

ERIK TOLLER

ACTA UNIVERSITATIS
UPSALIENSIS
2023

ISSN 1651-6214
ISBN 978-91-513-1905-6
urn:nbn:se:uu:diva-511929

UPPSALA
UNIVERSITET

Dissertation presented at Uppsala University to be publicly examined in Hambergsalen, Geocentrum, Villavägen 16, Uppsala, Thursday, 16 November 2023 at 10:00 for the degree of Doctor of Philosophy. The examination will be conducted in English. Faculty examiner: Professor James Craig (Department of Civil and Environmental Engineering, University of Waterloo, Waterloo, Ontario, Canada).

Abstract
Toller, E. 2023. Analytic Element Models for Groundwater Flow and Linear Elasticity in Fractured Rocks. *Digital Comprehensive Summaries of Uppsala Dissertations from the Faculty of Science and Technology* 2311. 86 pp. Uppsala: Acta Universitatis Upsaliensis. ISBN 978-91-513-1905-6.

There is an increasing demand for using deep underground space at various scales, such as small-scale geothermal wells and large-scale projects like tunnels or nuclear waste disposal. The deep underground space in fractured rock is a heterogeneous and challenging medium. Fractures have a significant impact on both the groundwater flow and the mechanical behavior. This thesis aims to develop analytic element models that capture the behavior of fractured rock for both groundwater flow and linear elasticity at different scales. Because these models are analytic in their formulation, they can model with machine precision and investigate behavior near singular points.

For groundwater flow, the thesis deals with two approaches to capture the groundwater flow behavior in fractured rock: a continuum approach and a discrete fracture network approach. The continuum approach considers the impact of fractures by varying the hydraulic conductivity based on depth. This method allows for efficient modeling while still capturing the depth-dependent behavior accurately. The discrete approach, in turn, implements the fractures directly by embedding them in the continuum. Unlike previous models, this model implements intersection without the need for approximations. The discrete model also demonstrates how fractures with discontinuous transmissivity are connected to model a heterogeneous fracture network.

For linear elasticity, the fractures and tunnels are modeled discretely in a plane strain continuum as analytic elements. These elements possess degrees of freedom, and no theoretical limitation exists on the number of elements. The execution of a model with 10,000 fractures effectively demonstrates the speed and accuracy of this method. Integrating seepage forces into the linear elastic model has improved the correlation between groundwater flow and linear elasticity. This enhancement allows for a more precise analysis of the impact of seepage forces near singular points. The solution's analytic formulation allows for the investigation of the behavior of the seepage force as a continuous function.

To conclude, a comparison between the analytic element model and a range of numerical methods reveals a strong agreement, with a mean error of less than 0.32%. The results demonstrate that the developed models are highly accurate and valuable tools for modeling fractured rocks.

Keywords: Analytic element method, fractures, tunnels, complex variables, linear elasticity, groundwater, fractured rock

Erik Toller, Department of Earth Sciences, LUVAL, Villav. 16, Uppsala University, SE-75236 Uppsala, Sweden.

ISSN 1651-6214
ISBN 978-91-513-1905-6
URN urn:nbn:se:uu:diva-511929 (http://urn.kb.se/resolve?urn=urn:nbn:se:uu:diva-511929)

Till min fru och mina barn, Julia, Edith & Ture

List of papers

This thesis is based on the following papers, which are referred to in the text by their Roman numerals.

I Toller, E.A.L., & Strack, O.D.L. (2019). Interface flow with vertically varying hydraulic conductivity. *Water Resources Research*, 55(11):8514-8525.

II Toller, E.A.L. (2022). An analytic element model for intersecting and heterogeneous fractures in groundwater flow. *Water Resources Research*, 58(5):e2021WR031520.

III Strack, O.D.L., & Toller, E.A.L. (2022). An analytic element model for highly fractured elastic media. *International Journal for Numerical and Analytical Methods in Geomechanics*, 46(2):297-314.

IV Toller, E.A.L., & Strack, O.D.L. (2023). An analytic element model for seepage forces in fractured media. *International Journal for Numerical and Analytical Methods in Geomechanics*, (submitted).

Contents

Abbreviations

AEM	Analytic Element Method
BEM	Boundary Element Method
DEM	Distinct/Discrete Element Method
DFN	Discrete Fracture Network
D-XFEM	Dual eXtended Finite Element Method
FDM	Finite Difference Method
FEM	Finite Element Method
FVM	Finite Volume Method
MFD	Mimetic Finite Difference
TPFA	Two-Point Flux Approximation

Variables

General

b^*	fracture width
z	complex variable, $z = x_1 + \mathrm{i}x_2$
i	complex number
L	fracture length
r_c	circle/tunnel radius
x_i	components of the Cartesian coordinate system $(i = 1,2,3)$
z_1, z_2	fracture endpoints
z_c	circle/tunnel center
γ	angle between the fracture and the x_1-axis

Groundwater Flow

$\tilde{B}$	width of the aquifer normal to the vertical plane
$\tilde{h}_f$	top of the saturated freshwater zone
$\tilde{h}_s$	bottom of the saturated freshwater zone
$\tilde{k}$	hydraulic conductivity (commonly also defined as K)
$\tilde{k}^*$	hydraulic conductivity of a fracture
$\tilde{Q}$	flow inside a fracture
$\tilde{Q}_{x_j}$	components of the discharge vector $(j = 1,2,3)$
$\tilde{q}_{x_j}$	components of the specific discharge vector $(j = 1,2,3)$
$\tilde{q}_n$	flow through a fracture
$\tilde{W}$	complex discharge function
$\tilde{\rho}_f$	density of freshwater
$\tilde{\rho}_s$	density of saltwater
$\tilde{\Phi}$	discharge potential
$\tilde{\phi}$	hydraulic head
$\tilde{\Psi}$	stream function
$\tilde{\Omega}$	complex potential

Linear Elasticity

B_0	body force
B_1	first integral of the body force
B_2	second integral of the body force
g	gravitational constant
p	pressure of a fracture
S	seepage force vector
T	traction
t_s, t_n	shear and normal component of the traction
u_{x_j}	component of displacement vector $(j = 1,2,3)$
w	complex displacement vector
ρ	density of rock
ρ_w	density of water
$\sigma_{x_j x_l}$	stress component $(j = 1,2,3, l = 1,2,3)$
τ^{11}	stress tensor component
τ^{12}	stress tensor component

Part I:
Introduction

1. Background

There is an increased demand for using the deep underground space for infrastructure projects, nuclear waste disposal, energy recovery, and mining. The underground space consists of highly heterogeneous rocks with fractures and faults and artificial structures such as tunnels, wells, and underground constructions. Figure 1.1 shows an underground space with various distinctive features.

The use of deep underground space ranges from, e.g., small-scale geothermal wells to large-scale, e.g., tunnels and nuclear waste disposal. There is an increased demand for tunnels that serve as shortcuts for traffic, power lines, and sewage disposal, and the tunnels provide a way of saving space in the natural and urban environments. Groundwater inflow into a tunnel may influence the surface level regarding water drawdown and ground deformations. To safeguard the surface from the harmful effects of a tunnel, it is crucial to thoroughly understand and model the processes related to tunnel inflow and its consequences in fractured rocks.

Utilizing the deep underground space is also essential for reaching the Sustainable Development Goals. According to Goldstein et al. (2011) can geothermal energy provide a long-term energy resource that is not likely to be affected by climate change. Sweden has more than 300,000 geothermal heat wells, according to Svergie Geologiska Undersökning (2023). Although most of these are for household production, geothermal energy has the potential even for large-scale heat and electric power production.

For some, groundwater is an essential part of everyday life. According to Livsmedelsverket (2023), more than one million people in Sweden use water from household wells. In a constantly changing climate, handling shared resources with care is essential. It is vital in areas with water scarcity, such as islands, where managing groundwater carefully becomes even more critical.

In order to gain a better understanding of how to treat the bedrock environment, it is necessary to conduct an investigation. Investigations provide valuable insights into the best approach to managing and maintaining the bedrock environment. Most of the information about the bedrock comes from drill cores and boreholes, which in volume only represent a small fraction of the space they investigate. Upscaling and extrapolating this data is a challenging task. It requires, among other things, models to interpret data and make predictions about the present and possible future conditions. The rock itself is a discontinuous, anisotropic, and inhomogeneous material. Jing (2003) adds that the rock is also a fractured porous medium containing fluids and gases.

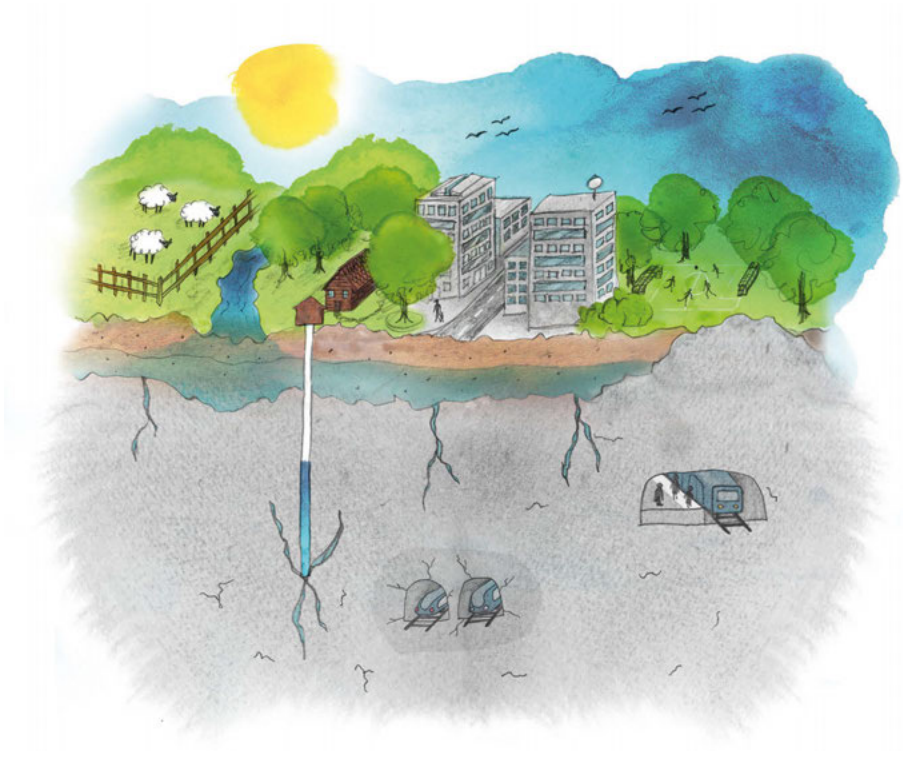

Figure 1.1. An illustration of the underground space and how it connects to the surface (Illustration printed with permission from Trafikverket).

Furthermore, a new ensemble of fractures emerges when excavating in rocks due to the excavation process.

Fractures are a critical feature in fractured rocks as they are the main paths for flow and transport and greatly influence mechanical behavior. These fractures vary in geometry and break up the rock mass, causing unique rock and groundwater mechanical properties. A large number of studies have addressed the groundwater flow and solute transport as well as mechanical properties in fractured rocks, e.g., (Nordqvist et al., 2008), (Zimmerman and Bodvarsson, 1996), (Kraemer, 1990), (Flemisch et al., 2018), (Hadgu et al., 2017), (Lei et al., 2017), (Bonnet et al., 2001), (Lei and Wang, 2016), (Harrison et al., 2002) and (Öhman and Niemi, 2003), to mention some.

One of the more significant challenges in fractured rocks is that the permeability typically is orders of magnitude greater in the fractures than in the rock mass. Thus, almost all groundwater flow is in the fracture network. Figure 1.2 illustrates how a fracture network may look at different scales, from the larger scale, where it is challenging to observe single fractures, down to the local scale, where the individual fractures are visible.

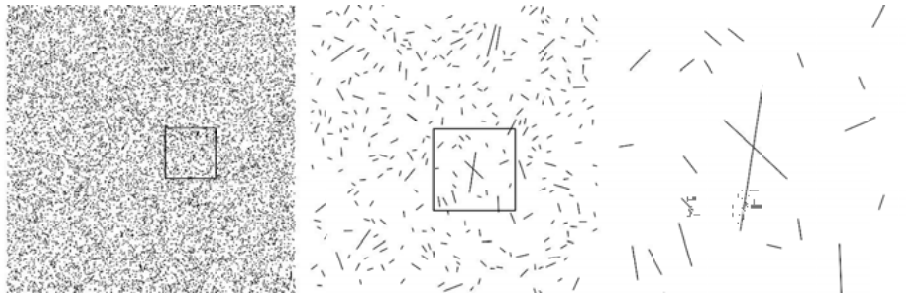

Figure 1.2. A fractured rock mass on different scales, the boundary of each panel corresponds to the box on the panel on its left.

Models are typically used to interpret the laboratory and field gap, and predict possible outcomes. As described by Jing (2003), going from the field to a model will involve subjective judgments. Not only is the interpretation of field data a source of uncertainty, but the choice of model will also have its strengths and limitations. Models provide an essential tool for understanding the deep underground space, and many different models and methods exist.

A significant challenge in the field is ensuring that the models represent reality. As the complexity and size of the models grow, uncertainties grow with them; there is a demand for a model with its accuracy independent of growth. A model should be accurate in both the large scale and in the details, as illustrated in Figure 1.2.

2. Modeling groundwater flow and mechanical processes in fractured rocks

Understanding fractured rocks and how to model them is a challenging task, and one contributing factor is the natural heterogeneity of fractures and faults. Another issue is that observations, e.g., boreholes, only cover parts of the fracture network. Converting limited knowledge into a general conclusion is difficult and often time-consuming. Models help with this challenging task with both interpretation and estimation of uncertainties.

2.1 Numerical models

The engineering fields addressing groundwater flow and rock mechanics use many numerical models. Standard numerical methods use approximate solutions for the governing partial differential equation. There are two common approaches in the formulation of the solution; one is by meshing the domain space, as in the Finite Element Method (FEM), Finite Volume Method (FVM), and Finite Difference Method (FDM), while the other is to formulate the boundary value problem on a boundary or particle, as in the Boundary Element Method (BEM), Distinct Element Method (DEM) and Analytic Element Method (AEM).

Using meshes FEM, FVM, and FDM can capture complex geometries and non-linear behavior. The main principle of FEM, FVM, and FDM is to formulate the partial differential equation as a linear or quadratic equation within an element or cell. As a result, the accuracy of the solution is dependent on the grid size. Local areas of interest typically use a more refined grid. There exist numerous textbooks on these methods, e.g., (Reddy, 2019), (Thomas, 2013), and (Mazumder, 2015).

Numerical methods for fractured rocks can, according to Jing (2003), be divided into three methods, continuum methods, e.g., FEM, FDM, and BEM, discontinuum methods, e.g., DEM, Discrete Fracture Networks (DFN), and hybrid continuum/discontinuum models, which are a combination of the two. According to Jing and Hudson (2002), the choice of method will be determined by the problem scale and density of fractures. Jing (2003) argues that the geometry of a rock mass can never be fully known, and thus, only part of a model can be verified or validated. Therefore, it is the task of all models to work with the uncertainties of the field data.

A continuum model has the benefit of being efficient in its calculations and suitable for larger domains. In a continuum model, the medium is described by a representative elementary volume, indicating that the properties are uniform. According to Bonnet et al. (2001), naturally fractured media may never fulfill this condition, which limits the use of continuum models significantly.

As stated in Kachanov (1993), anisotropic fractures are challenging for assigning the effective parameters for a mechanical continuum model. A significant challenge is that the displacements are discontinuous across fractures. The effective parameters are often estimated using empirical formulas, e.g., (Hoek and Brown, 1997) and (Sitharam et al., 2001). Singh (1973a,b) presented a mechanical continuum characterization method for fractured rocks. Singh (1973b) could show that the predicted values from the FEM model were in good agreement with the continuum model, except in areas with a steep stress gradient. Additionally, the model result showed that anisotropy has a more substantial impact when the shear modulus is low. Other techniques for continuum estimation are also discussed in Zimmerman (1990).

Fractures not only disrupt the displacements but also the groundwater flow. Although continuum models are efficient in modeling groundwater flow, they sometimes have difficulty meeting the requirements of a model, especially on a very local scale. A DFN model performs better for cases with a high demand for local variability. Niemi et al. (2000) showed that the continuum model can significantly underestimate the conductive characteristics and groundwater flow, which illustrated the need for DFN models. Not only may the continuum representation miss the local flow patterns, but it may also, in some instances, result in an incorrect flow. Öhman and Niemi (2003) addressed this issue by studying under which conditions a stochastic continuum approach, (Neuman, 1987), is applicable and introduced an oriented permeability correlation structure. Öhman and Niemi (2003) showed that it is possible to get accurate results using a continuum approach, but only for some cases. This technique was also later used in Öhman et al. (2005b). Another issue related to upscaling, raised by Öhman et al. (2005a), is that typically a vertical borehole is biased towards horizontal fractures. Öhman et al. (2005a) proposed a model incorporating the anisotropic rock stress in interpreting and scaling the borehole data.

In contrast to continuum models, a discrete model handles fractures accurately. However, the limitation is, according to Lei et al. (2017), the increased complexity of the models and the extensive data needs. The data available for the construction of these models are uncertain and limited. Consequently, there needs to be more certainty about whether the generated fracture network is a good representation of reality.

For many DFN models, the intact rock matrix is considered an impermeable boundary, e.g., (Neuman, 2005) and (Berkowitz, 2002). This assumption is often reasonable, especially when dealing with crystalline rocks, as in Nordqvist et al. (2008) and Zimmerman and Bodvarsson (1996). For a re-

view and comparison of numerical methods, see Flemisch et al. (2018) and Berre et al. (2021), who presents a collection of two-dimensional and three-dimensional DFN models.

The fracture network properties in fractured rocks are fundamentally three-dimensional. A challenge is that the measurements are often in one or two dimensions. For a deterministic fracture network model, it is challenging to accurately capture the geometry and connectivity of fractures when their properties are specifically assigned. A technique for dealing with this issue is the stochastic DFN approach, where the fractures and their properties follow some probabilistic distributions. Stochastic DFN approaches are well studied, e.g., concerning their connectivity (Bour and Davy, 1998) and (Bour and Davy, 1997), and effective parameters (Zimmerman and Bodvarsson, 1995) and (Min et al., 2004a). Niemi et al. (2000), Öhman and Niemi (2003), Öhman et al. (2005a), Huang et al. (2021) and Lei et al. (2017) provide many references for the stochastic approach.

Numerical methods can deal with the heterogeneity of fractured rocks, and there are many advances in numerical modeling of complicated geometries and fracture load conditions, e.g., (Kuna, 2013) and (Mohammadnejad et al., 2021). The continuum grid-based models, e.g., FEM, can deal with a varying continuum medium at a much higher frequency (cell-to-cell) than gridless models such as BEM and AEM. However, as described by Banks-Sills (1991), one of the difficulties with grid-based numerical methods is to capture the singular behavior near fracture tips. Furthermore, grid-based models have difficulty handling different scales within the model, so it is difficult to consider both the regional scale of fractured rocks and the behavior near fracture tips simultaneously.

2.2 Analytic solutions

Engineering modeling heavily relies on different properties, usually based on analytic solutions, often simplifying geometries but providing precise answers. Although they are highly accurate solutions, their usefulness could be improved. Nonetheless, they offer valuable insights into the factors that affect the solution's behavior, which other methods may not reveal.

The flow in a single fracture is typically represented by the flow between two parallel plates per unit width given by the cubic law, presented in Snow (1969). This solution is idealized and does not consider variation in aperture or surface roughness. Although many have developed different methods to deal with this, e.g., (He et al., 2021) and summarized by De Marsily (1986), the simplified geometries limit the use of the cubic law.

Examples of methods for upscaling and obtaining average properties for fractured rocks without explicitly modeling the fractures include the methods of Snow (1965) and Oda (1985). Snow (1965) derived a general permeability

tensor for a fracture network by adding the permeability tensors for each fracture. Oda's method is analytic and computes the equivalent permeability of fractures with arbitrary orientation; see Oda (1985). A significant limitation of these methods is that they assume that all fractures are connected.

To further improve the continuum model, Kitterød (2004), Şen (2014), and Şen (1989) use a varying continuum that accounts for the variation in hydraulic properties due to fractures. This variation can, for example, be depth-dependent, as shown in Ericsson and Ronge (1986). Such an adaptation limits the need for different layers to represent the changes in hydraulic properties and increases the efficiency and accuracy of the model.

A common approach when modeling rock mechanics is to assume that the rock is linearly elastic. A linearly elastic model is a mathematical model of how the stresses deform a solid object, and the stresses and strain are linearly dependent on each other. In linear elasticity, numerous analytic solutions exist for different features, e.g., (Muskhelishvili, 1953) and (Griffith, 1921). Muskhelishvili (1953) present the Muskhelishvili-Kolosov functions' which relate the stresses and strains in a general form for linearly elastic plane strain media. Griffith (1921) developed the exact solution for a pressurized fracture in an elastic medium under plane strain. Later, Irwin (1957) studied the behavior at crack tips closely based on the work by Inglis (1913), Griffith (1921), and Westergaard (1939). As explained in Perez (2017), studying fractures in rock mechanics is essential as they can lead to catastrophic failure without warning. This failure is sometimes desirable, as in hydraulic fracturing, but often undesirable and weakens the strength of the rock mass. These analytic solutions describe a simplified geometry and a single feature, e.g., fracture or tunnel.

Since Griffith (1921), the solution for a single fracture was later extended to other variations of fracture set-ups, e.g., (Westergaard, 1939), (Sneddon, 1946), (Sneddon and Elliot, 1946), (Sih, 1966) and (Gerolymatou, 2019), and a set of multiple fractures, e.g., (Benthem and Koiter, 1973), (Sneddon, 1973), and (Kachanov, 1993). Helsing (2000) presents a solution to many fractures, where the stress state of a medium containing 10,000 fractures is solved with high accuracy using the Fredholm integral equation.

There also exist fracture models using polynomials, like the method of pseudotraction, which were developed by Chudnovsky and Kachanov (1983), Horii and Nemat-Nasser (1985), Hori and Nemat-Nasser (1987), and Chudnovsky et al. (1987). The method of pseudotraction involves using truncated Taylor series to estimate the tractions on each fracture. This approach is inaccurate if the fractures are close to each other, particularly near the fracture tip. To overcome this limitation, Benveniste et al. (1989) proposed an approach to approximate polynomials using various base functions. They also approximated the fracture solved for as a single fracture within an infinite space, which was loaded by a specific traction. This specific traction included the contributions of all fractures.

One technique to solve linearly elastic boundary problems is the complex variable method. The principle of the complex variable method is to formulate the solution and boundary conditions in terms of complex variables, which enables the use of powerful mathematical techniques, e.g., series expansions and conformal mapping. These methods have been applied to both fractures, e.g., (Kusumoto et al., 2013), (Kusumoto and Gudmundsson, 2014) and (Leitman and Villaggio, 2005), and cavities, e.g., (Verruijt, 1997), (Zeng et al., 2019), (Strack and Verruijt, 2002), (Yu et al., 2014), (Fu et al., 2015) and (Fang et al., 2015), a general description is given in, e.g., (Muskhelishvili, 1953), and (Sadd, 2014). Common for these solutions is that they give an exact solution to a specific boundary value problem.

Even though analytic solutions are limited to simplified geometries, they still provide a good reference. For example, the equation for tunnel inflow from Gustafson (2009) is widely used in tunneling projects in Sweden, e.g., (Berzell, 2011), (Lissel, 2016), and (Svensson and Lissel, 2017, 2019). These projects use analytic solutions to first, in a simple and fast way, get a rough estimate of the tunnel inflow. The Gustafson (2009) method is a variation of Goodman et al. (1964) and calculates the inflow considering the damaged rock mass and the injection thickness. As shown by Svensson and Lissel (2017), this analytic solution tends to overestimate the inflow compared to numerical models. Stochastic calculations can help interpret the results by giving different probabilities of different cases, as demonstrated in Lissel (2016).

2.3 Analytic element models

This thesis will only briefly cover the background and theory (see chapter 4) of the Analytic Element Method. The interested reader can find more in the summary paper by Strack (2003) or in numerous textbooks, e.g., (Strack, 1989), (Haitjema, 1995), and (Strack, 2017).

The Analytic Element Method was first developed in the late 1970s and published in the early 1980s; see Strack and Haitjema (1981a), Strack and Haitjema (1981a), and Strack (1982). The first comprehensive summary of the method was given in the book Strack (1989). The method initially dealt with regional two-dimensional flow. However, it was later extended to transient flow, e.g., (Haitjema and Strack, 1985), (Zaadnoordijk, 1990), (Zaadnoordijk and Strack, 1993) and (Bakker, 2004), and three-dimensional flow, e.g., (Haitjema, 1985), (Fitts, 1989), (Jankovic et al., 2006) and (Fiori et al., 2006). It was also applied to large-scale models, such as the national groundwater model of the Netherlands, (De Lange, 1996, 2006), and the Yucca Mountain model in the US, (Bakker et al., 1999). Because the AEM is mesh-free, the model domain can grow without losing accuracy. Beginning with the textbook Strack (2020) and the articles in this thesis, AEM was also extended to linear elasticity.

The building blocks of the AEM are analytic elements. These elements are analytic functions that possess degrees of freedom. Many analytic elements can be combined using the principle of superposition to create more complex models where each element makes it possible to enforce a specific boundary condition, e.g., a constant hydraulic head or a discontinuity in the stream function.

Each analytic element expresses an analytic function typically as an infinite power series. This formulation means that the solution meets the differential equation exactly everywhere in the domain; the power series coefficients are determined to satisfy the condition on the element's boundary. Finding the coefficients is usually done using integrals, e.g., the Fourier or the Cauchy integral, or by solving linear equations. The truncation of the number of coefficients determines the degrees of freedom of the element.

A fundamental benefit of the AEM is that it does not discretize the domain, only along the element boundary. This property means that the solution is scale-independent. For instance, one model can accommodate numerous elements and be used on both micro and macro scales, as shown in Barnes and Janković (1999) and Strack and Toller (2022).

The AEM was previously used to model fracture flow with the first solution presented by Strack (1982). Steward (2015) presented a solution using thin inhomogeneities to model a large assembly of slits. Based on AEM van Harmelen and Weijermars (2018) present a solution for intersecting fractures. A key component for modeling fractures using AEM is the limitless analytic element developed by Strack (2018), which can handle a discontinuous behavior at the tip of a line element.

Strack (2020) first presented the analytic element for linearly elastic media based on a closed-form solution for gravity acting on a half-space. The papers attached to this thesis introduce the more general analytic element that introduces degrees of freedom. The AEM is similar to the complex variable method, which presents many closed-from solutions.

Jing (2003) writes that no closed-form solution exists for the geometries of the rock in Earth's upper crust. Although AEM is not a closed-form solution due to its infinite series, it comes close to it as it uses an analytic expression with infinite degrees of freedom. That is why AEM is helpful for benchmarking and validation.

2.4 Comparison of methods

Many modeling methods exist for both groundwater flow and linear elasticity. In Figure 2.1 are some of the most common numerical methods presented in terms of the number of publications per year that has the method as a key-

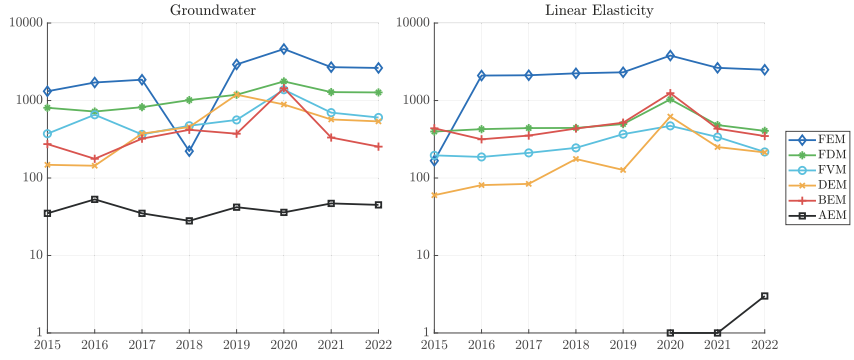

Figure 2.1. Number of publications in $\log_{10}$-scale per keyword for groundwater (left) and linear elasticity (right) between 2015 and 2022.

word[1]. This simple comparison illustrates that FEM dominates the scientific output for groundwater and linear elasticity. Kraemer (2007) also found a similar result when he studied groundwater models.

By examining Figure 2.1, it is clear that AEM has a lower publication rate than other methods. This result is likely because the community researching and using AEM is smaller than that for other numerical methods, and its models are not as widely utilized, resulting in smaller output. It is important to note that a higher output does not necessarily mean a better method but rather one that is more easily applicable. Nevertheless, the data suggest that numerical methods other than AEM have a faster pace of development.

When considering the applicability of the different methods, Craig and Read (2010) presents a helpful scale. This scale ranges from analytical to numerical solutions. The methods close to the analytical side indicate that they are mathematically more accurate, while those close to the numerical side provide a more flexible and adaptable method. This scale emphasizes that the capability to handle complex geometries is often a limiting factor for AEM. Although there has been some significant development in this, e.g., Strack (2018) enabled the creation of intersecting and connected features with higher accuracy. Nevertheless, AEM will always emphasize accuracy rather than detailed local variability. For situations where the variation is on the cell level, the FEM or other approximative methods are much better suited.

Omar et al. (2019) did a comparison study between the AEM, using the software AnAqSim, and FDM, using MODFLOW. The test case was the Lower Ganga River basin, where both models were set up and calibrated to the same data. Omar et al. (2019) found that the AEM model was more efficient and less difficult to set up. The AEM model also gives a more flexible approach to

[1]Source: `https://app.dimensions.ai/`, search with keywords: (numerical method) + "groundwater" or "linear elasticity", 2023-05-24

not well-defined boundary problems. On the other hand, the FDM approach is better if the problem has non-horizontal layers and heterogeneous permeability. Again, accuracy and speed must come at the cost of the need for model heterogeneity.

2.5 Coupled hydro-mechanical models

Natural phenomena are frequently a function of many different interacting processes. For rocks, these processes are, e.g., hydrological, mechanical, thermal, chemical, and more. These processes also depend on each other. For example, a stress change affects the aperture of a fracture and, thus, the permeability. Presented by Tsang (1987), sometimes a single process can answer a problem statement, while some problems require a coupled treatment of the processes. These coupled processes are either coupled one way or two ways. In this thesis, the coupling concerns the hydro-mechanical in one way.

A hydro-mechanical coupling is a link between the hydrological and mechanical processes of a fluid and a solid. According to Rutqvist and Stephansson (2003) and Wang (2000) there exist four different couplings:

1. A solid-to-fluid coupling occurs when a change in applied stress produces a change in fluid pressure or fluid mass.
2. A fluid-to-solid coupling occurs when a change in fluid pressure or fluid mass produces a change in the volume of the porous medium.
3. A solid-to-fluid coupling occurs when applied stress changes hydraulic properties.
4. A fluid-to-solid coupling occurs when a change in fluid pressure produces a change in mechanical properties.

The first two are direct couplings, and the last two are indirect couplings. In the case of fractured rocks, indirect couplings are the most common ones. Rutqvist and Stephansson (2003) provides an in-depth review on the topic of hydro-mechanical coupling in fractured rocks.

Many have studied the hydro-mechanical coupling for rocks. Some of these studies look at the effect the stresses have on the permeability of fractures and groundwater flow, e.g., (Tsang et al., 2018), (Figueiredo et al., 2015), (Fu et al., 2013) and (Ivars, 2006). Carlsson and Olsson (1977) showed the dependence between the hydraulic pressures and the stress state, as did Min et al. (2004b) and Zhang and Sanderson (1996). Min et al. (2004b) showed that permeability is more sensitive to stress change at low-stress levels than at high-stress levels.

When groundwater flows in a rock, it exerts a seepage force proportional to its gradient of the hydraulic head on the rock mass. In most cases, the seepage force is much weaker than the forces caused by pore or confining pressures, which typically leads to it being neglected. For some cases, however, it is crucial to consider. Lee and Nam (2001) demonstrates that it is essential to consider the pressures caused by the seepage force on a tunnel under a lake.

Previous studies have focused on investigating the impact of seepage forces on the stability of rock masses. Anagnostou and Kovári (1996) and Perazzelli et al. (2014) studied the tunnel face stability under a seepage force, a typical application. Pan and Dias (2018) and Lee and Nam (2001) examined the tunnel wall. Park et al. (2008) presented an analytic solution where the tunnel in a half-space is mapped to a disk in another plane; the solution included functions for both zero pressure and constant head.

Minkoff et al. (2003), studied fractures subjected to a seepage force and included only the flow in the fractures. Yan and Zheng (2017) presented a further development that also included the flow in the rock mass. Zhao et al. (2021) looked at the propagation of seepage forces in a water-injected fractured system. They showed that the seepage force increases close to fractures that draw water from the rock matrix.

A major gap in the current state-of-the-art is that no model can combine regional and small scale with analytic accuracy that extends beyond the model capacity of an exact solution. Although it is possible to determine the relative importance of seepage forces for a tunnel prior to this thesis, it is not possible to determine this with the same level of accuracy when combined with fractures.

3. Objective of the Thesis

This thesis aims to develop methods for understanding groundwater flow and stresses/deformations in fractured rocks. Developing analytic element models allows challenging geometries to be constructed and solved with machine precision. Due to their precision, they can be used as reference solutions and for investigating the influence of fractured rock properties. The ambition is to have a scale-independent fractured rock model with machine precision accuracy and no theoretical limit on the number of elements that could be included.

The thesis aims to create a model that analyzes groundwater flow and linear elasticity in fractured rocks using an analytic element model approach. The focus is on crystalline rocks with fractures embedded in the rock mass. This case requires accurate treatment of the rock mass and the discrete fractures, where the fractures include singularities at their tips. An analytic element model accurately handles the behavior along the fracture and at their tips.

The aim is to create several models that can either independently, or in combination, model the groundwater flow and certain rock mechanical processes on a large variety of scales, from the neighborhood of individual fractures to the combined effect of thousands of fractures. These models provide a tool that is a continuous link between the different scales; the objectives are to develop models that:

- efficiently consider the effect of fractures on regional groundwater flow (Paper I),
- provide an exact representation of fracture intersections (groundwater flow in Paper II, linear elasticity in Paper III), and
- can investigate the relative importance of seepage forces in a fractured medium (Paper IV).

Meeting all objectives, the project yields models helpful for understanding groundwater flow and rock mechanics in a fractured medium at both a regional and local scale.

The thesis follows a structured approach. Firstly, the theory is presented that is the foundation of the models. Next, the research results are presented, specifically the development of different models. The first two models are for groundwater flow, while the latter are for linear elasticity. A comparison is made and discussed to demonstrate how the developed models compare to existing ones.

Part II:
Theory Development

4. The Analytic Element Method

This chapter reviews some basic functions and theorems used in the Analytic Element Method. More detailed descriptions can be found in Strack (2020) and Strack (2003). The Analytic Element Method uses complex variable analysis, where the Cartesian (x_1, x_2)-space is written in terms of a single complex variable

$$z = x_1 + \mathrm{i}x_2. \tag{4.1}$$

A function that is a function of only this complex variable $f(z)$ is holomorphic. A holomorphic function is infinitely differentiable at each point z, except at singular points, and is also locally equal to its own Taylor series.

The functions presented in this thesis are either holomorphic inside or outside the unit circle. A function that is holomorphic inside the unit circle can be expanded into a Taylor series about the origin of the complex χ-plane:

$$f(\chi) = \sum_{n=0}^{\infty} a_n \chi^n \tag{4.2}$$

If a function is holomorphic outside the unit circle, it can be expanded into an asymptotic expansion about infinity, $\chi = 0$,

$$f(\chi) = \sum_{n=0}^{\infty} b_n \chi^{-n}. \tag{4.3}$$

For practical reasons, the series is truncated at a value N, which also represents the element's degrees of freedom. The boundary conditions determine these series' coefficients a_n and b_n.

A powerful mathematical technique in complex variables is conformal mapping. By using conformal mapping, a boundary in the z-plane can be mapped onto a boundary in another plane, where the boundary has a simpler shape, e.g., the unit circle. A common mapping is that of a circle in the z-plane onto the unit circle in the Z-plane, $Z = X + \mathrm{i}Y$, which is given by:

$$Z = \frac{z - z_c}{r_c} \tag{4.4}$$

where z_c and r_c are the center and radius of the circle. Another common mapping is a line between z_1 and z_2 in the z-plane onto a unit circle in the χ-plane defined by $\chi = \Re\chi + \mathrm{i}\Im\chi$. First, the line is mapped to the Z-plane as:

$$Z = \frac{2z - z_1 - z_2}{z_2 - z_1} \tag{4.5}$$

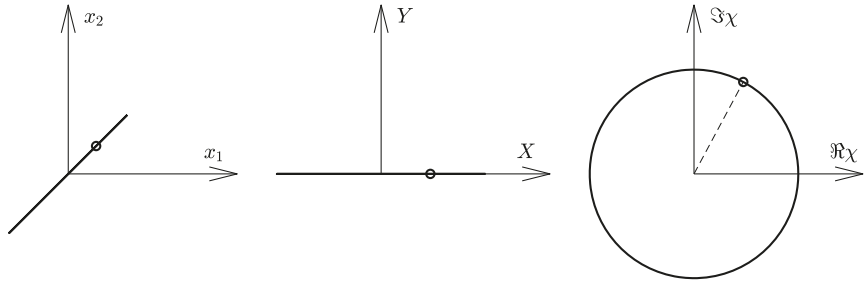

Figure 4.1. The mapping of a line in the z-plane to the unit circle in the χ-plane via the Z-plane.

where it maps onto a line of length two oriented along the X-axis. The mapping to the χ-plane is given by:

$$\chi = Z + \sqrt{Z-1}\sqrt{Z+1} \tag{4.6}$$

with two square roots. As explained in Strack (2020), two square roots are necessary. The inverse mappings are

$$Z = \frac{1}{2}\left(\chi + \frac{1}{\chi}\right) \tag{4.7}$$

and

$$z = \frac{1}{2}\left[Z(z_2 - z_1) + z_1 + z_2\right] \tag{4.8}$$

or in terms of the length, angle, and center point

$$z = \frac{1}{2} L Z e^{i\gamma} + z_0 \tag{4.9}$$

where L is the length of the line, γ is its angle to the x_1-axis and z_0 its center point. This mapping is illustrated in Figure 4.1.

This thesis has developed methods and solutions for the AEM for fractured rocks, focusing on groundwater flow in fractures, represented as a continuum and discrete fractures. It also presents a novel application of AEM for linear elasticity and the first coupled model for AEM. The models use superpositioning of analytic elements to create complex solutions, accurately handling the boundary conditions.

4.1 Groundwater flow

This thesis follows the formulation of Strack (2017). The equations consider flow in the plane defined by the Cartesian (x_1, x_2)-space. The continuum represents a rock with an isotropic hydraulic conductivity, governed by Darcy's

law such that

$$\tilde{q}_{x_1} = -\tilde{k}\frac{\partial\tilde{\phi}}{\partial x_1} \qquad \tilde{q}_{x_2} = -\tilde{k}\frac{\partial\tilde{\phi}}{\partial x_2} \tag{4.10}$$

where $\tilde{q}_{x_1}$ and $\tilde{q}_{x_2}$ are the components of the specific discharge vector, $\tilde{k}$ is the hydraulic conductivity and $\tilde{\phi}$ the hydraulic head. The complex discharge function $\tilde{W}$ is

$$\tilde{W} = \tilde{Q}_{x_1} - \mathrm{i}\tilde{Q}_{x_2} = -\frac{d\tilde{\Omega}}{dz} \tag{4.11}$$

where $\tilde{Q}_{x_1}$ and $\tilde{Q}_{x_2}$ are the two components of the discharge function, and $\tilde{\Omega}$ is the complex potential, which is holomorphic and a function of z only. The real and imaginary parts of the complex potential are the discharge potential $\tilde{\Phi}$ and the stream function $\tilde{\Psi}$

$$\tilde{\Omega} = \tilde{\Phi} + \mathrm{i}\tilde{\Psi}. \tag{4.12}$$

The discharge potential in terms of the hydraulic head for flow in the vertical plane is

$$\tilde{\Phi} = \tilde{k}\tilde{B}\tilde{\phi} \tag{4.13}$$

where $\tilde{B}$ is the width of the aquifer normal to the vertical plane.

For shallow unconfined flow Dupuit (1863) and Forchheimer (1886) proposed an approximation, the Dupuit-Forchheimer approximation, where the vertical variation of the hydraulic head $\tilde{\phi}$ is neglected, which implies that the vertical component of flow $\tilde{q}_{x_3}$ is neglected too. Somewhat similarly, Strack (1984) proposed that the vertical component $\tilde{q}_{x_3}$ exists but does not depend on the vertical variation of $\tilde{\phi}$

$$\tilde{q}_{x_3} \neq 0 \qquad \frac{\partial\tilde{\phi}}{\partial x_3} = 0. \tag{4.14}$$

Another way of approximating the total flow over the saturated thickness is by vertical integration:

$$\tilde{Q}_{x_1} = \int_0^{\tilde{h}} \tilde{q}_{x_1} dx_3 = -\tilde{k}\int_0^{\tilde{h}} \frac{\partial\tilde{\phi}}{\partial x_1} dx_3 \tag{4.15}$$

$$\tilde{Q}_{x_2} = \int_0^{\tilde{h}} \tilde{q}_{x_2} dx_3 = -\tilde{k}\int_0^{\tilde{h}} \frac{\partial\tilde{\phi}}{\partial x_2} dx_3, \tag{4.16}$$

where $\tilde{h}$ is the saturated thickness. The vertically integrated discharge and the Dupuit-Forchheimer approximation are equal for some boundaries. Charny (1951) showed that this is the case for a dam with vertical faces and a well in an unconfined aquifer. Paper I uses vertically integrated flow to model regional groundwater flow on a fractured bedrock with a saltwater interface.

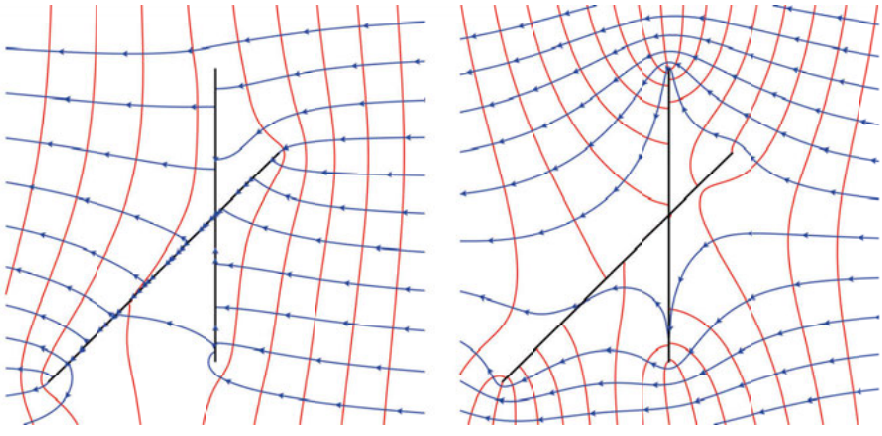

Figure 4.2. Flow around draining fractures (left) and blocking fractures (right), the blue lines with arrows represent the streamlines and the solid red lines the equipotentials.

4.1.1 Fracture flow

The rock may include discrete fractures, and then the flow in the fractures relates to the flow in the typically far less permeable rock mass. The fracture causes a jump in the hydraulic conductivity between the hydraulic conductivity in the continuum, $\tilde{k}$, and that of the fracture, $\tilde{k}^*$. This jump can either cause the fracture to draw water when $\tilde{k}^* > \tilde{k}$, which is called a draining fracture, or divert the groundwater flow when $\tilde{k}^* < \tilde{k}$, which is called a blocking fracture. Flow nets for draining fractures and blocking fractures in a field of uniform flow are shown in Figure 4.2. For this and all other flow nets, the blue lines with arrows represent the streamlines, and the solid red lines are the equipotentials.

A draining fracture causes a discontinuity in the stream function $\tilde{\Psi}$; the discontinuity equals the flow $\tilde{Q}$ in the fracture

$$\tilde{\Psi}^+ - \tilde{\Psi}^- = -\tilde{Q} \qquad \tilde{\Phi}^+ = \tilde{\Phi}^- \tag{4.17}$$

where the $+$ and $-$ denote the two sides of the fracture. The stream function jumps, but the discharge potential is continuous across the fracture. For a blocking fracture, the discharge potential $\tilde{\Phi}$ is discontinuous across the fracture, but the stream function is continuous

$$\tilde{\Phi}^+ - \tilde{\Phi}^- = \tilde{\lambda} \qquad \tilde{\Psi}^+ = \tilde{\Psi}^-. \tag{4.18}$$

A key component for using the AEM for modeling fracture flow is the limitless analytic element developed by Strack (2018). The element is written either in terms of the line-doublet

$$\underset{db}{\tilde{\Omega}} = \frac{1}{2\pi \mathrm{i}} \sum_{n=0}^{\infty} a_n F_n \tag{4.19}$$

which has a real part that jumps and an imaginary part that is constant, or as the line-dipole

$$\underset{dp}{\tilde{\Omega}} = \frac{1}{2\pi} \sum_{n=0}^{\infty} b_n F_n \tag{4.20}$$

which has an imaginary part that jumps and a constant real part. The function F_n is given by:

$$F_n = \left[\chi^n + \frac{1}{\chi^n} \right] \ln \frac{\chi - 1}{\chi + 1} + p_n(\chi) \tag{4.21}$$

where $p_n(\chi)$ is the far-field correction polynomial. The complex discharge functions of the line-doublet and line-dipole are

$$\underset{db}{\tilde{W}} = -\frac{d\underset{db}{\tilde{\Omega}}}{dz} = -\frac{2\chi^2 e^{-i\gamma}}{\pi L(\chi^2 - 1)} \sum_{n=0}^{\infty} a_n F_n' \tag{4.22}$$

and

$$\underset{dp}{\tilde{W}} = -\frac{d\underset{dp}{\tilde{\Omega}}}{dz} = -\frac{2\chi^2 e^{-i\gamma}}{\pi L(\chi^2 - 1)} \sum_{n=0}^{\infty} b_n F_n'. \tag{4.23}$$

The jump across the analytic element is given by the jump of the function $F_n(\chi)$

$$\begin{aligned} &\Delta F_n = F_n(\chi) - F_n(\bar{\chi}) = \\ &\left[\chi^n + \frac{1}{\chi^n} \right] \ln \frac{\chi - 1}{\chi + 1} + p_n(\chi) - \left[\bar{\chi}^n + \frac{1}{\bar{\chi}^n} \right] \ln \frac{\bar{\chi} - 1}{\bar{\chi} + 1} - p_n(\bar{\chi}) \end{aligned} \tag{4.24}$$

or

$$\Delta F_n = 2i\pi \cos(n\theta) \qquad \chi = e^{i\theta}. \tag{4.25}$$

The jump is non-zero at the tip of the element, i.e., $\theta = 0, \pi$, meaning it can handle the discontinuous behavior at the tip of the element. Paper II uses this property of a non-zero jump at the tips to model the intersection of the fractures by using multiple limitless analytic elements that meet at the point of intersection.

4.2 Linear elasticity

Linear elasticity relates the stresses to the strains and applies to many materials, e.g., rock, soil, and steel. In three dimensions, the strain and stresses are completely described for a point with the displacement vector and the stress tensor, given as:

$$u_{x_j} = [u_{x_1}, u_{x_2}, u_{x_3}] \tag{4.26}$$

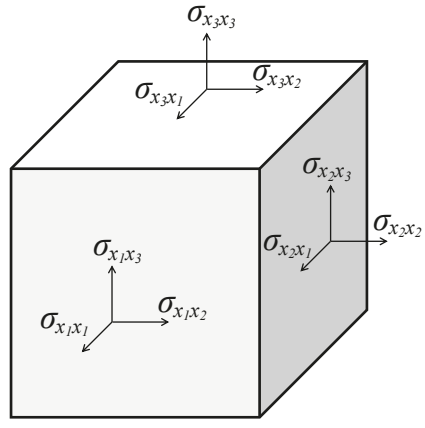

Figure 4.3. The components of the stress tensor in three dimensions.

and

$$\sigma_{x_j x_l} = \begin{bmatrix} \sigma_{x_1x_1} & \sigma_{x_1x_2} & \sigma_{x_1x_3} \\ \sigma_{x_2x_1} & \sigma_{x_2x_2} & \sigma_{x_2x_3} \\ \sigma_{x_3x_1} & \sigma_{x_3x_2} & \sigma_{x_3x_3} \end{bmatrix}. \tag{4.27}$$

The stress tensor components can be seen in Figure 4.3. Hooke's law, in combination with the equilibrium equations, gives a solution for the relation between the stresses and strains. Strack (2020) presents a general solution for the complex displacement vector and the two components of the stress tensor.

Strack (2020) developed a formulation for the complex displacements operating on a plane angled at an angle ζ to the x_1-direction as:

$$w = u_{x_1} - \mathrm{i}u_{x_2} = \frac{\mathrm{e}^{\mathrm{i}\zeta}}{4G}\left\{-\bar{z}\Phi'(z) + \kappa\bar{\Phi}(\bar{z}) + \Psi(z) - 2(1-2\nu)\bar{B}_2\right\} \tag{4.28}$$

where u_{x_1} and u_{x_2} are the components of the displacement vector in Cartesian (x_1, x_2)-space, Φ and Ψ are complex functions and B_2 is the second integral of the body force. Furthermore, Strack (2020) express the contra-variant components of the stress tensor in non-Cartesian $(\bar{z}, z)$-space as:

$$\tau^{11} = \bar{z}\Phi''(z) - \Psi'(z) \tag{4.29}$$

and

$$\tau^{12} = -\Phi'(z) - \bar{\Phi}'(\bar{z}) + \bar{B}_1 + B_1. \tag{4.30}$$

The expressions of τ^{11} and τ^{12} in terms of the Cartesian components, $\sigma_{x_1x_1}$, $\sigma_{x_2x_2}$, and $\sigma_{x_1x_2}$, of the stress tensor are

$$\tau^{11} = \sigma_{x_1x_1} - \sigma_{x_2x_2} - 2\mathrm{i}\sigma_{x_1x_2} \tag{4.31}$$

and

$$\tau^{12} = \sigma_{x_1x_1} + \sigma_{x_2x_2}. \tag{4.32}$$

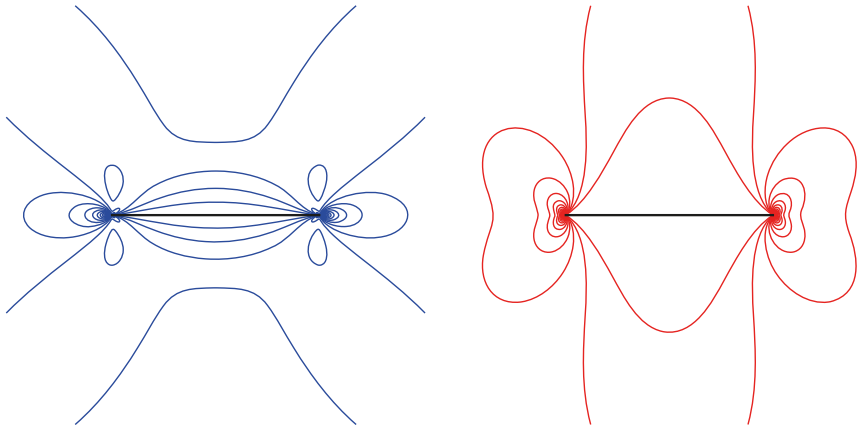

Figure 4.4. Contours of the major principal stress (right) and the minor principal stress (left) for a single fracture in a linearly elastic medium.

The complex form of the traction operating on a plane angled at an angle ζ to the x_1-direction is given by:

$$T = t_s - \mathrm{i}t_n = -\frac{1}{2}\mathrm{i}(\tau^{11}\mathrm{e}^{2\mathrm{i}\zeta} - \tau^{12}) \tag{4.33}$$

where t_s and t_n are the shear and normal components of the traction. The traction, or stress vector, is the force per unit area acting on a plane.

4.2.1 Pressurized fractures

Fractures cause a discontinuity in the stress and displacement field. A pressurized fracture creates a pressure that acts normal to the fracture surface. A fracture subjected to a normal force causes a Mode I stress intensity factor; see Irwin (1957) and Rice et al. (1968). Such fractures cause a square root singular behavior near the tip of the fracture, as shown in Figure 4.4.

AEM initially provided a solution for a uniformly pressurized fracture oriented along the x_1-axis in Strack (2020). It assumes normal pressure to the fracture surface and zero shear component. In terms of traction, this is

$$T = t_s - \mathrm{i}t_n = \mathrm{i}p \tag{4.34}$$

and the tractions are continuous across the fracture. Paper III uses this condition to develop an analytic element model for a highly fractured elastic medium.

4.2.2 Seepage force

This thesis studies the effect of seepage forces on the stress tensor. Flowing groundwater exerts a seepage force on the medium due to the pressure gradient

and is proportional to it. Large gradients occur, for example, around tunnels and near highly conducting fractures; Paper IV illustrates this.

The seepage force is a body force that affects both the complex displacements (4.28) and the isotropic stress tensor (4.30). The seepage force in complex form is

$$S = s_{x_1} - \mathrm{i}s_{x_2} = 2\rho_w g \frac{\partial \tilde{\phi}}{\partial z} \tag{4.35}$$

where s_{x_1} and s_{x_2} are the components of the seepage force in Cartesian (x_1, x_2)-space, ρ_w is the density of water and g is the gravitational constant. The body force B_0, in this thesis, is a combination of the seepage force and gravity:

$$B_0 = \rho g \left[\frac{\rho_w}{\rho} \frac{1}{\tilde{k}} \frac{d\tilde{\Omega}}{dz} + \mathrm{i} \right] \tag{4.36}$$

where ρ is the density of rock and $\tilde{\Omega}$ is the complex potential for groundwater flow. The two integrals of the body force in τ^{12} (4.30) and w (4.28) are

$$B_1 = \rho g \left[\frac{\rho_w}{\rho} \frac{1}{\tilde{k}} \tilde{\Omega} + \mathrm{i}z \right] \tag{4.37}$$

and

$$B_2 = \rho g \left[\frac{\rho_w}{\rho} \frac{1}{\tilde{k}} \int \tilde{\Omega} dz + \frac{\mathrm{i}z^2}{2} \right]. \tag{4.38}$$

The body force will represent the effect of seepage and gravity in the linearly elastic model. This thesis only considers a fluid-to-solid coupling and assumes that the steady-state groundwater model is unaffected by the linearly elastic model. Paper IV uses the body force to develop a model that accounts for seepage force and gravity in tunnels and fractures.

Part III:
Results

5. Interface flow with vertically varying hydraulic conductivity (Paper I)

Toller, E.A.L., & Strack, O.D.L. (2019). Interface flow with vertically varying hydraulic conductivity. *Water Resources Research*, 55(11):8514-8525.

Paper I, Toller and Strack (2019), regards the development of a continuum model for fractured rocks. Rather than modeling the fractures discretely, the hydraulic conductivity continuously varies with depth. This approach captures some general properties of fractures, such as the closing of fractures with depth, the distribution of fracture density, and the related decrease in hydraulic conductivity. This property is crucial for islands with a saltwater interface and large head gradients close to the coast. It is possible to model the aquifer as a multilayer, e.g., (Strack and Ausk, 2015). That approach would require many layers for cases with considerable variation, increasing the computational cost.

The function of the vertically varying hydraulic conductivity in Paper I is

$$\tilde{k}(x_3) = \tilde{k}_0 \mathrm{e}^{x_3/\tilde{\xi}} \tag{5.1}$$

where x_3 is the vertical coordinate, positive upward, of an (x_1, x_2, x_3) Cartesian coordinate system, $\tilde{k}_0$ is the hydraulic conductivity at sea level, and $\tilde{\xi}$ is a parameter of dimension length. Ericsson and Ronge (1986) showed that this expression for the hydraulic conductivity matched well with the field measurements in crystalline rocks.

Following Strack et al. (2006), the discharge potential is expressed as the integral of the discharge vector, defined as the vertically integrated specific discharge. The vertically integrated flow is

$$\tilde{Q}_{x_j} = -\int_{\tilde{h}_s}^{\tilde{h}_f} \tilde{k}(x_3) \frac{\partial \tilde{\phi}(x_1, x_2, x_3)}{\partial x_j} dx_3 \tag{5.2}$$

where $j = 1, 2$ and $\tilde{h}_s$ and $\tilde{h}_f$ are the bottom and top of the saturated freshwater zone measured from sea level. Using Leibniz's rule for differentiation, this

expression becomes

$$\tilde{Q}_{x_j} = -\frac{\partial}{\partial x_j}\int_{\tilde{h}_s}^{\tilde{h}_f} \tilde{k}(x_3)\tilde{\phi}(x_1,x_2,x_3)dx_3 \tag{5.3}$$
$$+\tilde{k}(\tilde{h}_f)\tilde{\phi}(x_1,x_2,\tilde{h}_f)\frac{\partial \tilde{h}_f}{\partial x_j} - \tilde{k}(\tilde{h}_s)\tilde{\phi}(x_1,x_2,\tilde{h}_s)\frac{\partial \tilde{h}_s}{\partial x_j}.$$

The integration gives the discharge potential for unconfined flow:

$$\tilde{\Phi} = \int_0^{\tilde{h}_f} \tilde{k}(x_3)\tilde{\phi}(x_1,x_2,x_3)dz - \frac{1}{2}\tilde{K}(\tilde{h}_f) \tag{5.4}$$

where

$$\tilde{K}(x_3) = 2x_3\int_0^{x_3} \tilde{k}(x_3)dx_3 - 2\int_0^{x_3}\int_0^{x_3} \tilde{k}(x_3)dx_3dx_3. \tag{5.5}$$

For a saltwater interface flow, the discharge potential also includes the lower boundary of the saturated zone and is

$$\tilde{\Phi} = \int_{\tilde{h}_s}^{\tilde{h}_f} \tilde{k}(x_3)\tilde{\phi}(x_1,x_2,x_3)dx_3 - \frac{1}{2}\left[\tilde{K}(\tilde{h}_f) + \frac{1}{\tilde{\alpha}}\tilde{K}(\tilde{h}_s)\right] \tag{5.6}$$

where

$$\tilde{\alpha} = \frac{\tilde{\rho}_f}{\tilde{\rho}_s - \tilde{\rho}_f}. \tag{5.7}$$

Using (5.1) the function $K(x_3)$ is

$$\tilde{K}(x_3) = 2x_3\int_0^{x_3} \tilde{k}_0 e^{x_3/\tilde{\xi}}dx_3 - 2\int_0^{x_3}\int_0^{x_3} \tilde{k}_0 e^{x_3/\tilde{\xi}}dx_3dx_3 \tag{5.8}$$

or

$$\tilde{K}(x_3) = 2\tilde{k}_0(x_3 - \tilde{\xi})\tilde{\xi}e^{x_3/\tilde{\xi}} + 2\tilde{k}_0\tilde{\xi}^2. \tag{5.9}$$

In Paper I, a comparison is made between the depth of the saltwater interface for a varying hydraulic conductivity and a constant one. It shows that the interface always will be higher with a vertically varying hydraulic conductivity where the hydraulic conductivity decreases with depth, meaning a higher risk for saltwater contamination. The results emphasize the importance of accurately capturing the vertical variation of the hydraulic conductivity for interface flow.

Paper I presents a case study involving the rocky island Brattö, fed by rainfall, and an analytic element model that considers the island's varying hydraulic conductivity. Figure 5.1 displays the resulting steady state hydraulic head for Brattö. The investigated problem was finding the maximum pumping rates of a set of wells with the condition that they do not draw salt water. All the wells were assumed to pump at a discharge such that the saltwater interface was just beneath the bottom of the well. It is evident from the results that the maximum pumping rate depends on the initial groundwater head and topography.

Figure 5.2 presents both a cross-section of Brattö and the hydraulic conductivity as a function of depth. Observing the two plots, it is noticeable that a large portion of the freshwater body is in a low hydraulic conductivity zone, where $x_2 < -500$ m. Flow in a low conductivity zone further emphasizes the need for properly implementing the variation of the hydraulic conductivity as it will significantly impact the availability of fresh water.

The results demonstrate that it is possible to include the effect of fracture behavior with depth within a continuum model. Identifying the precise location of fractures can be challenging, making excluding this information helpful. However, using this approach, the model still considers the overall behavior of fractures even if we do not know their specific properties.

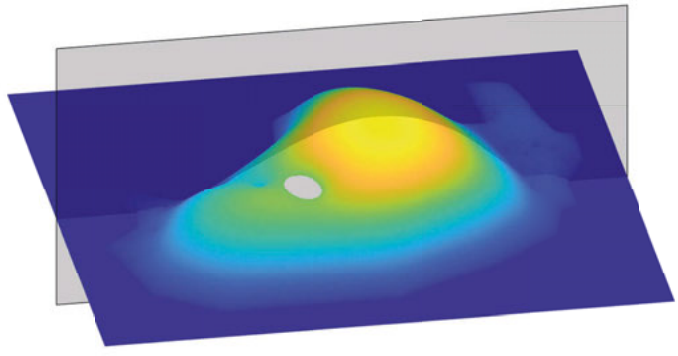

Figure 5.1. Hydraulic head over the island Brattö where the filled rectangle indicates the cross-section displayed in Figure 5.2.

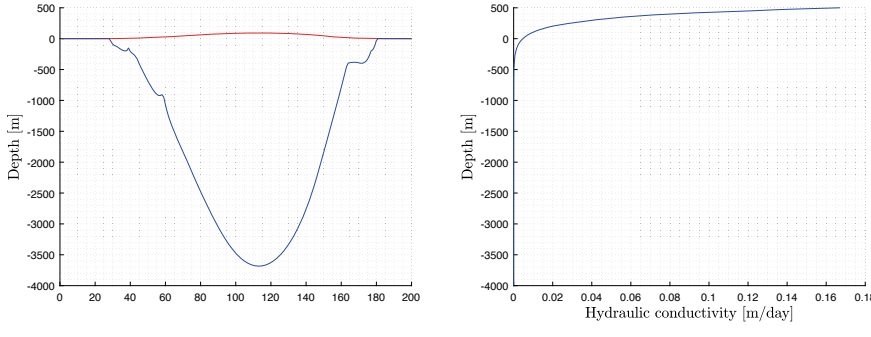

Figure 5.2. Cross section of the simulated hydraulic head and saltwater interface for Brattö (corresponding to surface indicated in Figure 5.1) (left) and the variation of hydraulic conductivity with depth (right).

6. An analytic element model for intersecting and heterogeneous fractures in groundwater flow (Paper II)

Toller, E.A.L. (2022). An analytic element model for intersecting and heterogeneous fractures in groundwater flow. *Water Resources Research*, 58(5):e2021WR031520.

Paper II, Toller (2022), contains the development and application of an analytic element model for intersecting and heterogeneous fractures in groundwater flow. A limiting factor in earlier AEM models of fractured rocks has been that the fractures were not allowed to intersect without approximating the intersection, e.g., (Strack, 1982) and (Steward, 2015). Paper II provided the necessary development for a more accurate model of intersections in AEM without approximations. The same approach is also applicable to model jumps in transmissivity along fractures.

Multiple papers have studied analytic models for groundwater flow in intersecting fractures, e.g., (van Harmelen and Weijermars, 2018), (Khanal and Weijermars, 2019, 2020) and (Weijermars and Khanal, 2019). Flemisch et al. (2018) presents a benchmark study of numerical models, and the approach presented in Paper II is compared to this benchmark study later in this thesis (chapter 9).

The methodology presented in Paper II uses limitless analytic elements, see Strack (2018), and formulates the boundary conditions for both draining and blocking fractures. The fracture is represented by a line in the z-plane at an angle γ to the x_1-axis and length L, which is mapped onto the unit circle in the χ-plane via the Z-plane, see (4.5) and (4.6). The draining fracture uses the line-dipole (4.20) and the blocking fracture the line doublet (4.19).

The boundary condition for a draining fracture is derived by expressing Darcy's law in terms of the tangential component of the complex discharge vector, $\Re\{\tilde{W}e^{i\gamma}\}$, along the fracture. Similarly, the boundary condition for a blocking fracture is derived by expressing Darcy's law in terms of the normal component of the complex discharge vector, $\Im\{\tilde{W}e^{i\gamma}\}$, to the fracture. The boundary conditions are expressed in terms of the variables shown in Figure 6.1 where $\tilde{k}^*$ is the hydraulic conductivity of the fracture, b^* is the fracture width, ds is an incremental step along the fracture, $\tilde{\phi}_1$ and $\tilde{\phi}_2$ are the hydraulic heads at a distance ds from each other within the fracture, $\tilde{\phi}^+$ and $\tilde{\phi}^-$ are the hydraulic heads on the two sides of the fracture, $\tilde{Q}$ is the flow in the fracture and $\tilde{q}_n$ is the flow through the fracture.

The total flow in a fracture is calculated using Darcy's law (4.10) with

$$\tilde{Q} = -\tilde{k}^* b^* \frac{d\tilde{\phi}}{ds} \tag{6.1}$$

and expressed in terms of the discharge potential

$$\tilde{Q} = -\frac{\tilde{k}^* b^*}{\tilde{k}} \frac{d\tilde{\Phi}}{ds}. \tag{6.2}$$

This expression, combined with (4.17) and in terms of the complex discharge function, gives the boundary condition for a draining fracture as:

$$\Re\{\tilde{W} e^{i\gamma}\} = -\frac{\tilde{k}}{\tilde{k}^* b^*}(\tilde{\Psi}^+ - \tilde{\Psi}^-). \tag{6.3}$$

Similarly, the flow through a blocking fracture, $\tilde{q}_n$, is

$$\tilde{q}_n = \frac{\tilde{k}^*}{b^*}(\tilde{\phi}^+ - \tilde{\phi}^-) \tag{6.4}$$

or expressed in terms of the discharge potential

$$\tilde{q}_n = \frac{\tilde{k}^*}{\tilde{k} b^*}(\tilde{\Phi}^+ - \tilde{\Phi}^-). \tag{6.5}$$

This expression, combined with (4.18) and in terms of the complex discharge function, gives the boundary condition for a blocking fracture as:

$$\Im\{\tilde{W} e^{i\gamma}\} = \frac{\tilde{k}^*}{\tilde{k} b^*}(\tilde{\Phi}^+ - \tilde{\Phi}^-). \tag{6.6}$$

Paper II uses the line-dipole function (4.20) to model the draining fracture. The jump in the imaginary part (4.25) combined with the boundary condition gives:

$$\Re\{\tilde{W} e^{i\gamma}\} = -\frac{\tilde{k}}{\tilde{k}^* b^*} \sum_{n=0}^{\infty} b_n \cos(n\theta) \qquad \chi = e^{i\theta}. \tag{6.7}$$

The total complex discharge function is

$$\tilde{W} = \underset{dp}{\tilde{W}} + \underset{\text{others}}{\tilde{W}} \tag{6.8}$$

where $\underset{dp}{\tilde{W}}$ is the element that is being solved for and $\underset{\text{others}}{\tilde{W}}$ is the contribution from all other elements. Using (4.23), the expression for the unknown coefficients for a draining fracture is

$$\sum_{n=0}^{\infty} b_n \left[\Re\left\{ \frac{2\chi^2}{\pi L(\chi^2 - 1)} F_n' \right\} - \frac{\tilde{k}}{\tilde{k}^* b^*} \cos(n\theta) \right] = \Re\left\{ \underset{\text{others}}{\tilde{W}} e^{i\gamma} \right\} \tag{6.9}$$

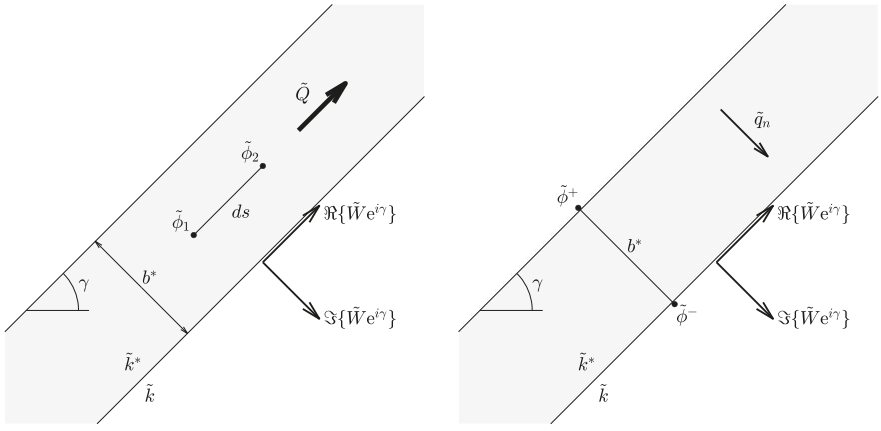

Figure 6.1. Illustration of the boundary conditions for a draining (left) and blocking fracture (right) (modified from Toller (2022)).

Similarly, the expression for the unknown coefficients for a blocking fracture is

$$\sum_{n=0}^{\infty} a_n \left[\Im \left\{ \frac{2\chi^2}{\pi \mathrm{i} L(\chi^2-1)} F_n' \right\} + \frac{\tilde{k}^*}{\tilde{k} b^*} \cos(n\theta) \right] = \Im \left\{ \underset{\text{others}}{\tilde{W}} \, \mathrm{e}^{\mathrm{i}\gamma} \right\} \tag{6.10}$$

where they are models using the line-doublet (4.19).

Rather than having continuous elements, an intersection uses four elements that meet at the point of intersection. For a draining fracture, the condition for the intersection is continuity of flow, while for a blocking fracture, it is continuity of the hydraulic head. These conditions are illustrated in Figure 6.2 and are expressed for $t = 1, \ldots, T$ elements meeting at the intersection as:

$$\sum_{t=1}^{T} (\underset{t}{\tilde{\Phi}}^+ - \underset{t}{\tilde{\Phi}}^-) = \sum_{t=1}^{T} \tilde{\lambda}_t = 0 \tag{6.11}$$

for blocking fractures where $\tilde{\lambda}$ is the jump in potential across the fracture and

$$\sum_{t=1}^{T} (\underset{t}{\tilde{\Psi}}^+ - \underset{t}{\tilde{\Psi}}^-) = -\sum_{t=1}^{T} \tilde{Q}_t = 0 \tag{6.12}$$

for draining fractures.

The same approach can be used to model jumps in transmissivity, where a jump will separate the fracture into two elements. The conditions are the same as for the intersection, but only two elements meet at the intersection point rather than four. The condition is defined by (6.11) and (6.12).

The method uses over-specification to solve for the unknown coefficients and implements the intersection conditions in the same solver. The solution takes into account the conditions both along the element and at the intersection at the same time.

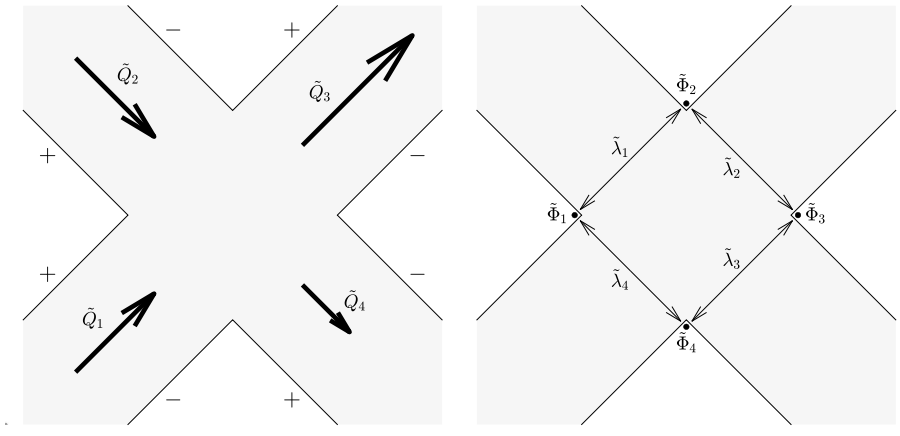

Figure 6.2. The intersection condition for draining (left) and blocking fractures (right) (modified from Toller (2022)).

Unlike many numerical DFN models, in this AEM model, the fractures are embedded in the continuum (rock matrix) and interact with the flow within the continuum. As a result, the continuum can host flow between the fractures, and between fractures and other elements, such as tunnels. Also, because the model gives all the local variables at every point, it provides an excellent tool for investigating the influences from fractures and fracture intersections.

Figure 6.3 presents the pressure contour for a fractured rock with a tunnel in a uniform flow field. This model combines both discontinuities in transmissivity in the fractures and at the intersection of fractures. The tunnel drains water and has zero pressure on the tunnel wall. The tunnel's drainage affects the pressure contours, and the surrounding fracture network affects the extent of the pressure drop. The presence of steep gradients reveals the effect of discontinuities in transmissivity, and the continuous contour lines demonstrate the continuity of the hydraulic head.

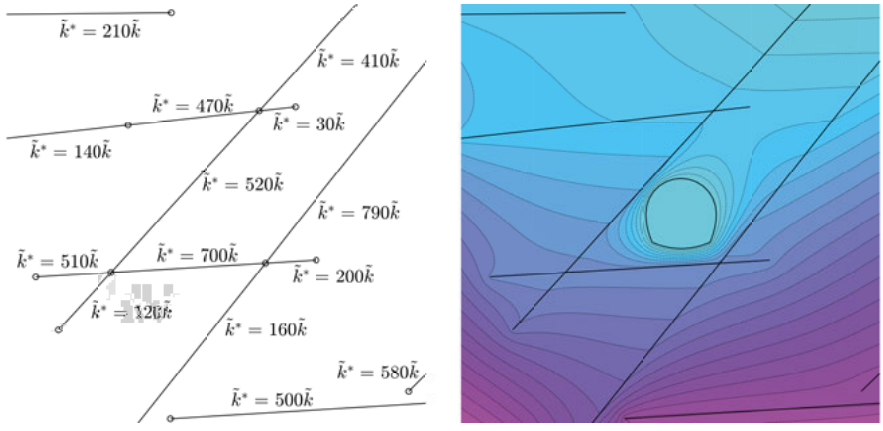

Figure 6.3. Fracture network surrounding a tunnel where the circles mark the endpoints of the elements (left) and the pressure contour (right) (reprint from Toller (2022)).

7. An analytic element model for highly fractured elastic media (Paper III)

Strack, O.D.L., & Toller, E.A.L. (2022) An analytic element model for highly fractured elastic media. *International Journal for Numerical and Analytical Methods in Geomechanics*, 46(2):297-314.

Paper III, Strack and Toller (2022), presents the development of an analytic element model for highly fractured elastic media. An extensive background on linear elasticity and AEM can be found in the textbook by Strack (2020). The functions presented in Paper III allow the fractures to intersect and have degrees of freedom. The equations used in this paper are equivalent to the Muskhelishvili-Kolosov functions'; see Muskhelishvili (1953). The fractures are assumed to have constant pressure, length L, angle γ to the x_1-axis, plane strain conditions, and maps to the unit circle in the χ-plane.

The fracture is expressed in terms of the components of the stress tensor, (4.29) and (4.30) excluding the body force, using (4.9) as:

$$\tau^{11} = \frac{1}{2} L \mathrm{e}^{-\mathrm{i}\gamma} \bar{Z} \Phi''(z) + \bar{z}_0 \Phi''(z) - \Psi'(z) \tag{7.1}$$

and

$$\tau^{12} = -\Phi'(z) - \bar{\Phi}'(\bar{z}). \tag{7.2}$$

Two new functions, ψ and ϕ, are introduced, defined by:

$$\Psi(z) = \frac{1}{2} L \mathrm{e}^{-\mathrm{i}\gamma} Z \Phi'(z) + \bar{z}_0 \Phi'(z) + \mathrm{e}^{-\mathrm{i}\gamma} \psi(z) \tag{7.3}$$

and

$$\phi = \mathrm{e}^{-\mathrm{i}\gamma} \Phi \tag{7.4}$$

with the derivative

$$\Psi'(z) = \mathrm{e}^{-\mathrm{i}\gamma} \phi'(z) + \frac{1}{2} L Z \phi''(z) + \bar{z}_0 \mathrm{e}^{\mathrm{i}\gamma} \phi''(z) + \mathrm{e}^{-\mathrm{i}\gamma} \psi'(z) \tag{7.5}$$

such that τ^{11} becomes

$$\tau^{11} = -\frac{1}{2} L (Z - \bar{Z}) \phi''(z) - \mathrm{e}^{-\mathrm{i}\gamma} \phi'(z) - \mathrm{e}^{-\mathrm{i}\gamma} \psi'(z) \tag{7.6}$$

which results in a function where the dependence on the two complex variables Z and $\bar{Z}$ vanishes along the fractures. The traction expressed in terms of these functions are

$$\begin{aligned} & t_s - \mathrm{i}t_n = \\ & -\frac{1}{2}\mathrm{i}\left\{-\frac{1}{2}L\mathrm{e}^{2\mathrm{i}\gamma}(Z-\bar{Z})\phi''(z) - \mathrm{e}^{\mathrm{i}\gamma}[\phi'(z)+\psi'(z)] + \mathrm{e}^{\mathrm{i}\gamma}\phi'(z) + \mathrm{e}^{-\mathrm{i}\gamma}\bar{\phi}'(\bar{z})\right\} \\ & = \frac{1}{2}\mathrm{i}\left\{\frac{1}{2}L\mathrm{e}^{2\mathrm{i}\gamma}(Z-\bar{Z})\phi''(z) + \mathrm{e}^{\mathrm{i}\gamma}\psi'(z) - \mathrm{e}^{-\mathrm{i}\gamma}\bar{\phi}'(\bar{z})\right\}. \end{aligned} \tag{7.7}$$

The traction along the element becomes

$$t_s - \mathrm{i}t_n = \frac{1}{2}\mathrm{i}\left\{\mathrm{e}^{\mathrm{i}\gamma}\psi'(z) - \mathrm{e}^{-\mathrm{i}\gamma}\bar{\phi}'(\bar{z})\right\}. \tag{7.8}$$

The two functions ϕ and ψ represent the analytic element. These functions are holomorphic outside the unit circle with the asymptotic expansions:

$$\phi = \sum_{n=1}^{\infty} \alpha_n \chi^{-n}, \tag{7.9}$$

and

$$\psi = \sum_{n=1}^{\infty} \beta_n \chi^{-n}. \tag{7.10}$$

These equations are valid for a fracture with a discontinuity of the displacement. The benefit of these elements is the correct handling of both the boundary conditions along the fracture and the singularity at the tip. The derivatives of these functions are

$$\phi' = \frac{d\phi}{dz} = -\sum_{n=1}^{\infty} n\alpha_n \frac{\chi^{-(n-1)}}{\chi^2-1}\frac{4}{L}\mathrm{e}^{-\mathrm{i}\gamma}, \tag{7.11}$$

$$\psi' = \frac{d\psi}{dz} = -\sum_{n=1}^{\infty} n\beta_n \frac{\chi^{-(n-1)}}{\chi^2-1}\frac{4}{L}\mathrm{e}^{-\mathrm{i}\gamma} \tag{7.12}$$

and

$$\phi'' = \frac{d^2\phi}{dz^2} = \sum_{n=1}^{\infty} n\alpha_n \frac{16}{L^2}\mathrm{e}^{-2\mathrm{i}\gamma}\frac{\chi^{2-n}}{(\chi^2-1)^3}\left[(n+1)\chi^2 - n + 1\right]. \tag{7.13}$$

The unknown coefficients α_n and β_n are related to each other via the condition of continuity of tractions, which gives

$$\begin{aligned} & t_s^+ - \mathrm{i}t_n^+ - \left(t_s^- - \mathrm{i}t_n^-\right) = \\ & -\frac{2\mathrm{i}}{L}\left[\frac{\chi}{\chi^2-1}\sum_{n=1}^{\infty} n(\beta_n\chi^{-n} + \bar{\alpha}_n\chi^n) - \frac{\bar{\chi}}{\bar{\chi}^2-1}\sum_{n=1}^{\infty} n(\beta_n\bar{\chi}^{-n} + \bar{\alpha}_n\bar{\chi}^n)\right] = 0 \end{aligned} \tag{7.14}$$

With $\chi\bar{\chi} = 1$ along the boundary, this simplifies to

$$\frac{\chi}{\chi^2 - 1} \sum_{n=1}^{\infty} [n\beta_n(\chi^n + \chi^{-n}) + n\bar{\alpha}_n(\chi^n + \chi^{-n})] = 0 \tag{7.15}$$

which gives

$$\alpha_n = -\bar{\beta}_n. \tag{7.16}$$

The expressions of the shear and normal components of the traction along the unit circle in the χ-plane, where $\chi = e^{i\theta}$, gives the coefficients β_n as:

$$t_s = -\frac{2}{L\sin(\theta)} \sum_{n=1}^{\infty} n\Im\beta_n \sin(n\theta) \tag{7.17}$$

and

$$t_n = -\frac{2}{L\sin(\theta)} \sum_{n=1}^{\infty} n\Re\beta_n \sin(n\theta). \tag{7.18}$$

The expression for t_s and t_n guarantees that all elements' contributions to the traction along the fracture give $t_s = 0$ and $t_n = -p$.

The analytic element model allows extensive fracture sets in a linearly elastic medium. Paper III presents the stress trajectories for 10,000 fractures under a uniform horizontal stress field, Figure 7.1 and 7.2. Because of the formulation of the analytic element, the solution is valid for any point in the medium. This method opens up the possibility of looking at the combined effect from a theoretically unlimited number of fractures while also being able to look at the stresses at machine precision close to the singular tip. Figure 7.1 and 7.2 also demonstrate that it is possible to model intersecting fracture, as is seen as we zoom in to the intersecting fracture set in Figure 7.2.

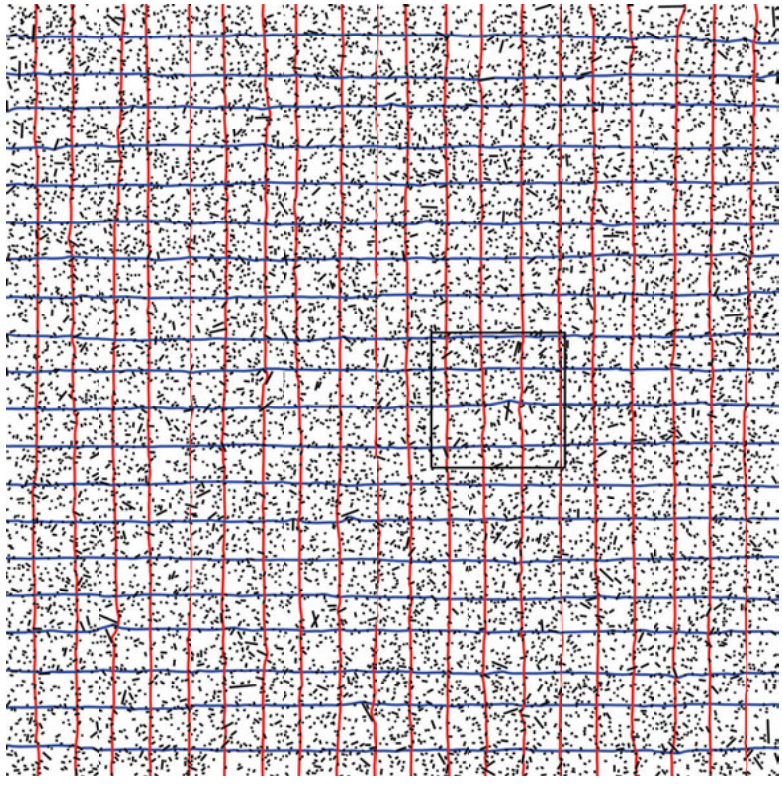

Figure 7.1. Trajectories of the major principal stresses (blue lines) and the minor principal stresses (red lines), for 10,000 cracks in a linearly elastic medium (reprint from Strack and Toller (2022)).

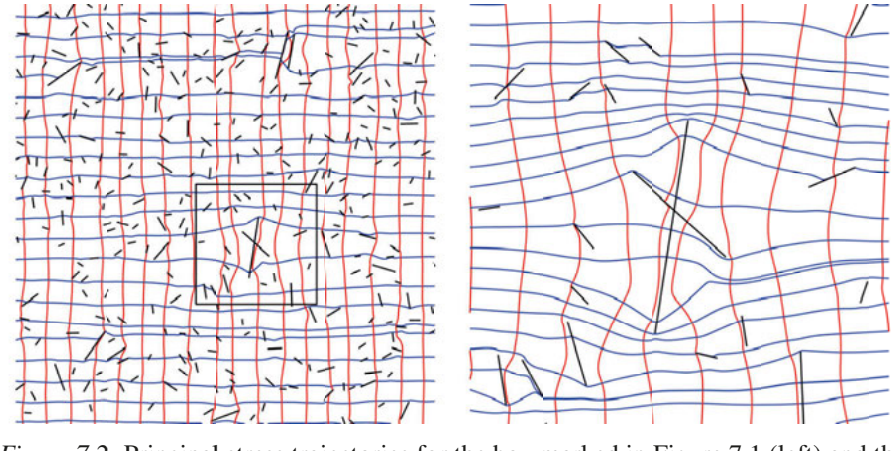

Figure 7.2. Principal stress trajectories for the box marked in Figure 7.1 (left) and the principal stress trajectories for the box marked in the left panel (right) (reprint from Strack and Toller (2022)).

8. An analytic element model for seepage forces in fractured media (Paper IV)

Toller, E.A.L., & Strack, O.D.L. (2023). An analytic element model for seepage forces in fractured media. *International Journal for Numerical and Analytical Methods in Geomechanics*, (submitted).

Paper IV, Toller and Strack (2023), covers the inclusion of seepage forces in the linearly elastic model for fractured media. While Paper III treated fractures in elasticity without including the body forces, Paper IV included the body force due to seepage and gravity.

The initial part of Paper IV involves the development of the analytic element for a tunnel, including the seepage forces. The solution for the analytic element uses (4.37) and expresses the traction components along the unit circle in the Z-plane. The tensor components for the tunnel element are given by:

$$\tau^{11} = r_t \left(\bar{Z} - \frac{1}{Z} \right) \Phi''(z) - \psi'(z) \tag{8.1}$$

and

$$\tau^{12} = -\Phi'(z) - \bar{\Phi}'(\bar{z}) + \bar{B}_1(\bar{z}) + B_1(z). \tag{8.2}$$

The traction is expressed along the unit circle in the Z-plane and two new holomorphic functions, P and Q, are introduced that relate to Φ', ψ' and the traction as:

$$\Phi' = Q - P, \tag{8.3}$$

$$\psi' = 2PZ^{-2}, \tag{8.4}$$

$$\Im P = t_s \quad Z\bar{Z} = 1 \tag{8.5}$$

and

$$\Re Q = t_n + \frac{1}{2}[B_1(z) + \bar{B}_1(\bar{z})] \quad Z\bar{Z} = 1. \tag{8.6}$$

The new functions are expanded in terms of the asymptotic series

$$P = \sum_{n=0}^{\infty} a_n Z^{-n} \tag{8.7}$$

and

$$Q = \sum_{n=0}^{\infty} b_n Z^{-n}. \tag{8.8}$$

By utilizing holomorphic matching, similar to Strack (2009), and expanding the tunnel element's function into an asymptotic expansion, the following Cauchy integrals provide solutions for the unknown coefficients:

$$a_n = -\frac{\mathrm{i}}{\pi} \int_{-\pi}^{\pi} t_s \mathrm{e}^{\mathrm{i}n\theta} d\theta \tag{8.9}$$

and

$$\bar{b}_n = -\frac{1}{\pi} \int_{-\pi}^{\pi} (t_n + \Re B_1)\, \mathrm{e}^{\mathrm{i}n\theta} d\theta. \tag{8.10}$$

Paper IV also presents an analytic element for a fracture with the body forces. The solution is similar to that in Paper III, except that the normal traction component is also a function of the body force (4.37)

$$\tau^{11} = -\frac{1}{2} L (Z - \bar{Z})\, \phi''(z) - \mathrm{e}^{-\mathrm{i}\gamma} \phi'(z) - \mathrm{e}^{-\mathrm{i}\gamma} \psi'(z) \tag{8.11}$$

and

$$\tau^{12} = -\mathrm{e}^{-\mathrm{i}\gamma} \phi'(z) - \mathrm{e}^{-\mathrm{i}\gamma} \bar{\phi}'(\bar{z}) + \bar{B}_1(\bar{z}) + B_1(z). \tag{8.12}$$

The traction along the element is

$$t_s - \mathrm{i}t_n = \frac{1}{2}\mathrm{i} \left[\mathrm{e}^{\mathrm{i}\gamma} \psi'(z) - \mathrm{e}^{-\mathrm{i}\gamma} \bar{\phi}'(\bar{z}) + \bar{B}_1(\bar{z}) + B_1(z) \right]. \tag{8.13}$$

The functions for ϕ and ψ are written as asymptotic expansions

$$\phi = \sum_{n=1}^{\infty} \alpha_n \chi^{-n} \tag{8.14}$$

and

$$\psi = \sum_{n=1}^{\infty} \beta_n \chi^{-n}. \tag{8.15}$$

The relationship between α_n and β_n is based on the continuity of tractions, similar to (7.14), and is identical to that given in Paper III. Because the real part of the body force is constant across the fracture, it vanishes from the expression. Hence, the solution for the coefficients of the asymptotic expansions is identical, except for the body force term.

The contribution of the two components of the body force to the isotropic stress mainly depends on the hydraulic head and the elevation, as seen in (4.37). Because the density of rock is higher than that of water, $\rho > \rho_w$, the contribution due to gravity will, in many cases, dominate, especially at depth, given that the groundwater level is on or below the surface. Figure 8.1 presents the flow net for a tunnel in a uniform flow field and the contribution to

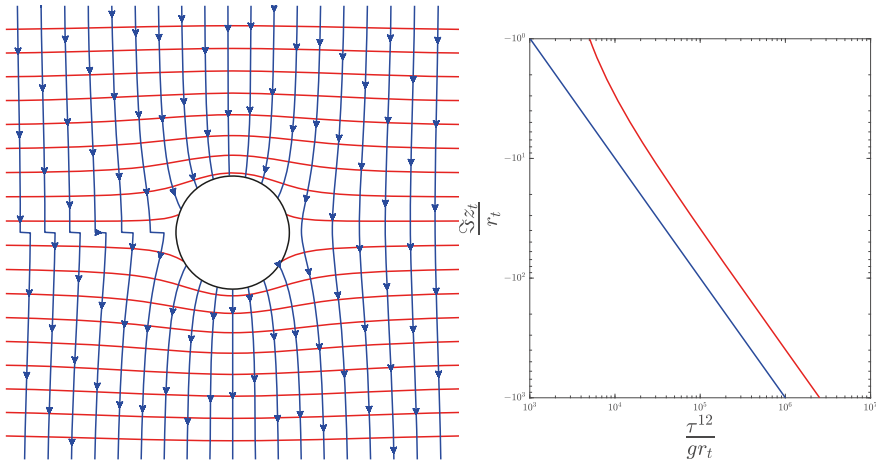

Figure 8.1. The flow net for a tunnel in a field of uniform flow (left) and the two body force components (right), seepage force (blue), and gravity (red), contribution to the isotropic stress as a function of depth (reprint from Toller and Strack (2023)).

the isotropic stress τ^{12} of the two components of the body force. The discontinuity in the stream function in the flow net is due to the branch cut from the tunnel element. A branch cut is a jump in the imaginary part of the complex potential over a line caused by the jump in the argument of the logarithm.

A case where the seepage force is higher than the contribution from gravity is when the complex potential has an additional hydraulic head added, e.g., a fracture beneath a lake or under artesian pressure. Presented in Figure 8.2 is the flow net of a single fracture in a field of uniform flow and the contribution of the seepage and gravity to the isotropic stress as a function of distance from the upper fracture tip projected along the x_1-axis. The figure shows that the influence on the isotropic stress from seepage decreases as a function of distance away from the fracture.

A key advantage of the analytic element model is that it allows for any combination of analytic elements. Unlike other analytical solutions, e.g., (Park et al., 2008), this model can combine both tunnels and fractures. Figure 8.3 presents the $\log_{10}$ contour of the deviatoric stress for a combined model with both a tunnel and a fracture set in a field of uniform flow under a constant hydraulic head. As shown in Figure 8.3, the influence of the fractures on the deviatoric stress is significant and important to consider.

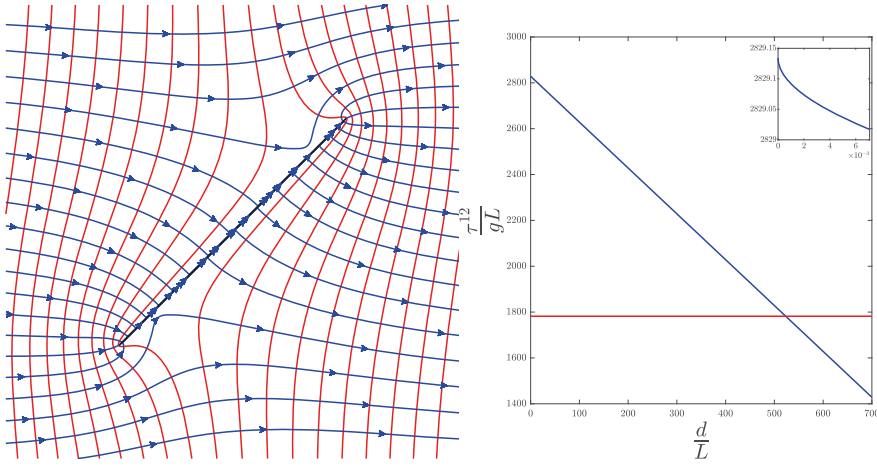

Figure 8.2. The flow net for a fracture in a field of uniform flow (left) and a plot of the contributions to the isotropic stress form the two components of the body force (right), seepage force (blue) and gravity force (red), as a function of distance computed along a line parallel to the x_1-axis beginning at the upper right fracture tip (reprint from Toller and Strack (2023)).

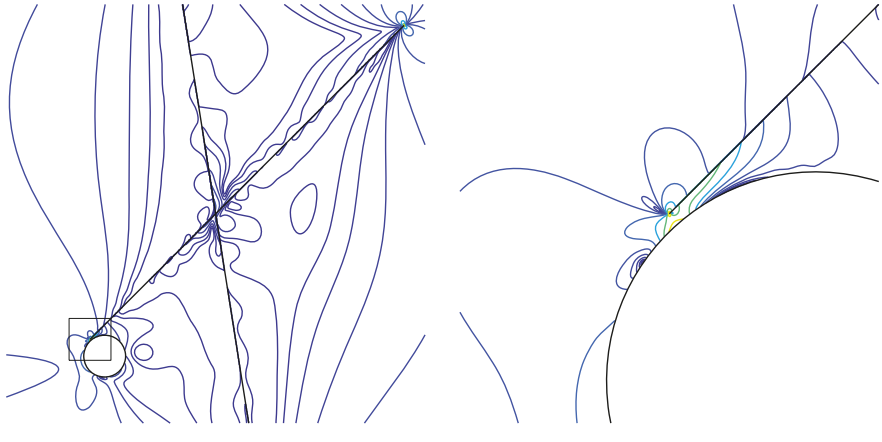

Figure 8.3. Contour of the deviatoric stress in $\log_{10}$ scale for a tunnel and a fracture set in a field of uniform flow under a constant hydraulic head, the boundary of the right panel corresponds to the box on the left panel (reprint from Toller and Strack (2023)).

9. Benchmark study

This chapter compares the developed AEM model to a published benchmark study by Flemisch et al. (2018) where a number of numerical models for fracture flow were compared to each other and against reference benchmark cases. The benchmark 3 for intersecting fractures is modeled here. The model consists of ten fractures, involving draining and blocking fractures, inside a box where two sides are impermeable, and two sides have a constant hydraulic head. The geometry of the problem is presented in Figure 9.1 and is a replica of Benchmark 3 from Flemisch et al. (2018). The red lines (1-3,6-10) are draining fractures, the blue lines (4-5) are blocking fractures, the solid black lines are impermeable boundaries, the dotted black lines are constant head boundaries, and the dashed black line is the arc where the hydraulic heads are compared between the models. In one case, the flow goes from top to bottom; in the other, the flow is from left to right.

Because the boundaries of AEM are at infinity, the treatment of boundary conditions differs from other numerical methods. The reference solution uses the Mimetic Finite Differences (MFD), see Brezzi et al. (2005) and Flemisch and Rainer (2008), with a fine grid for the fractures and the continuum. The reference solution, in this case, is a numerical simulation. Following the problem definition, the AEM model uses the parameters given in Table 9.1. The results are presented in terms of hydraulic head and hydraulic conductivity.

Figure 9.2 compares results from the AEM model and those of other methods as presented in Flemisch et al. (2018) for benchmark 3 in terms of the hydraulic head along the arc shown in Figure 9.1. Flow is from left to right. The result of the AEM model fall within the range of the other models and is actually closer to the reference solution than most of the other models in the case of flow from left to right. The most significant discrepancy between the reference solution and the AEM model is the handling of the discontinuity when crossing the blocking fractures in the case of flow from left to right.

The two solutions closest to the reference solution are the Flux-Mortar and the Two-Point Flux Approximation (TPFA). The Flux-Mortar models the fractures as interfaces between the cells and mixes the FEM with the Mortar method, see Boon et al. (2018). The mortar space, or the space between non-matching elements, allows Darcy flow and is coupled with the surrounding flow. More on mortar space can be read in Arbogast et al. (2000). The TPFA, see Karimi-Fard et al. (2004), is an FDM that uses a two-point flux approximation. It evaluates the fluxes between cells based on the cells' center pressure and the face transmissibility. The TPFA* in Flemisch et al. (2018) is a modification of the TPFA where the fracture intersection cells are kept intact.

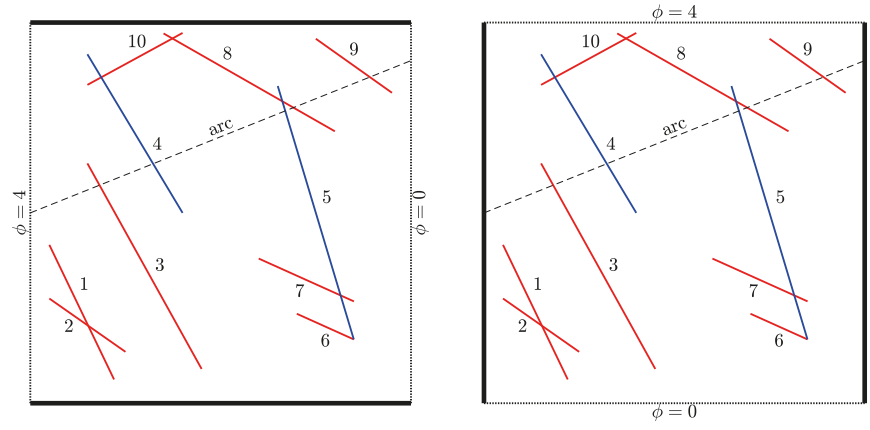

Figure 9.1. The model set-up for Benchmark 3, flow left to right (left) and flow top to bottom (right), the red lines are draining fractures, and the blue lines are blocking fractures (modified from Flemisch et al. (2018)).

$\tilde{k}$	=	1	hydraulic conductivity (continuum)
$\tilde{k}^*$	=	10^4	hydraulic conductivity (draining fractures)
$\tilde{k}^*$	=	10^{-4}	hydraulic conductivity (blocking fractures)
b^*	=	10^{-4}	aperture of fractures
m	=	20	number of coefficients (blocking fractures)
m_{far}	=	600	number of far-field coefficients (blocking fractures)
m	=	10	number of coefficients (draining fractures)
m_{far}	=	200	number of far-field coefficients (draining fractures)
m	=	20	number of coefficients (constant head elements)
m_{far}	=	600	number of far-field coefficients (constant head elements)

Table 9.1. *The input data for the AEM model.*

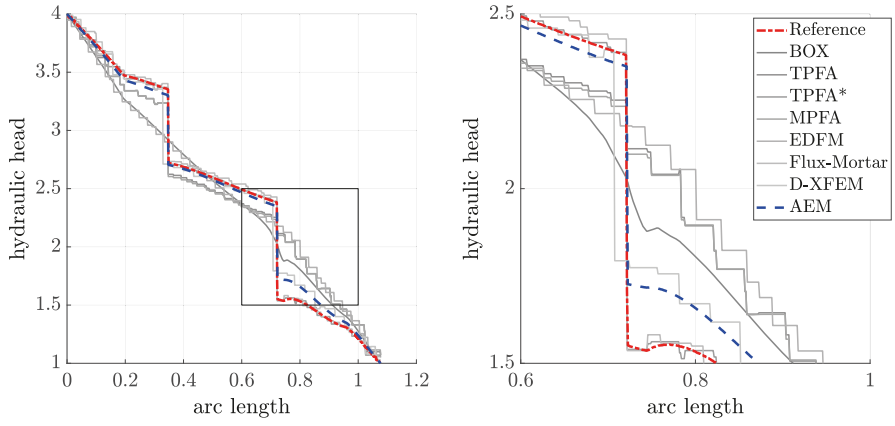

Figure 9.2. Comparison of the AEM model results to results of the methods presented in benchmark 3 in Flemisch et al. (2018), where the flow is from left to right. The right panel's boundary corresponds to the black box's boundary on the left panel.

The solution most similar to AEM, in Figure 9.2, is the D-XFEM which is dual extended FEM, see D'Angelo and Scotti (2012). Like the Flux-Mortar method, it also deals with the fracture flow by including it in a mortar space. The D-XFEM, however, allows for the fractures and porous mesh to be non-matching, and a cell intersected by a fracture divides it into smaller components.

The ability to model flow through a blocking fracture is visible in the other part of Benchmark 3, flow from top to bottom. Figure 9.3 compares the AEM model to the other methods in this case. The hydraulic head jump vastly differs between AEM and all other methods when crossing the blocking fracture on the right (see arc length 0.7 to 0.75). The difference is that in the AEM model, the draining fracture transfers the flow through the fractures and discharges it on the other side of the blocking fracture, while the numerical methods take the harmonic average of the transmissivity at the intersection.

Figure 9.4 presents the difference in head between the reference solution and the AEM model for the two cases. The difference between the AEM model and the reference model is calculated at each point using

$$\Delta\tilde{\phi} = \left| \frac{\tilde{\phi}_{\text{AEM}} - \tilde{\phi}_{\text{MFD}}}{\tilde{\phi}_{\text{MFD}}} \right|. \tag{9.1}$$

The reference solution was interpolated to a matching grid of the AEM model to compare the two models. When comparing contours, it is clear that the largest difference in hydraulic head is around the intersection of a blocking and draining fracture.

All numerical methods in Flemisch et al. (2018) that can explicitly account for the effect of fracture transmissivity at the intersection of the draining and

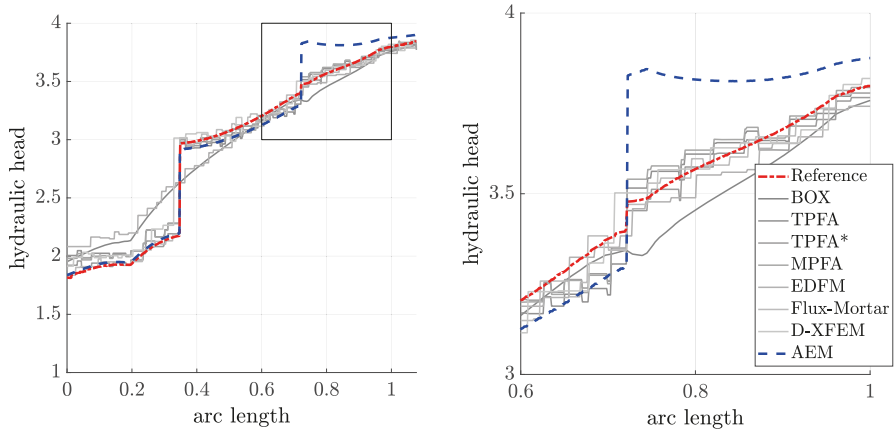

Figure 9.3. Comparison of the AEM model results to results of the methods presented in benchmark 3 in Flemisch et al. (2018), where the flow is from top to bottom. The right panel's boundary corresponds to the black box's boundary on the left panel.

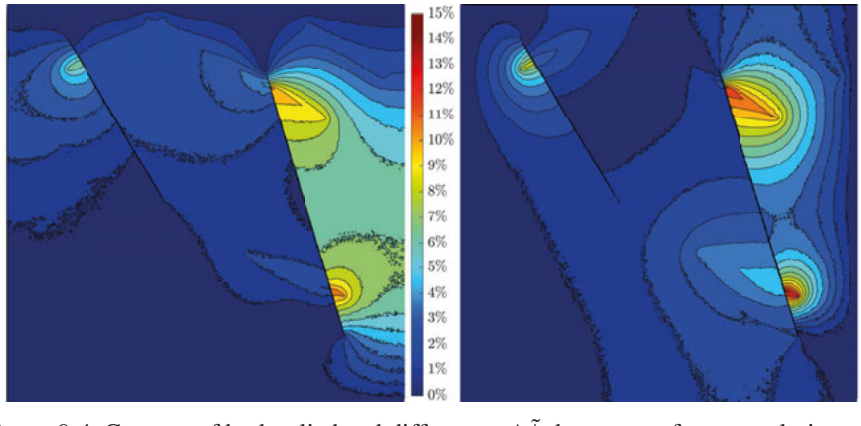

Figure 9.4. Contour of hydraulic head difference, $\Delta\tilde{\phi}$, between reference solution and the AEM model for flow left to right (left) and flow top to bottom (right).

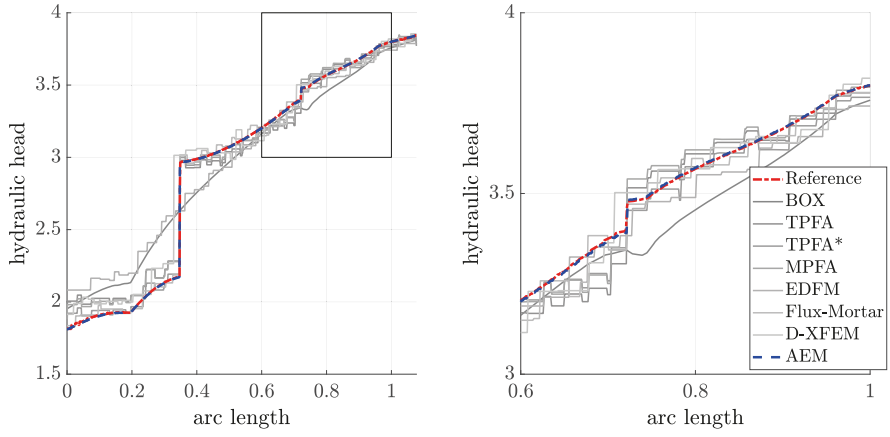

Figure 9.5. Comparison of the modified AEM model results to results of the methods presented in benchmark 3 in Flemisch et al. (2018), where the flow is from top to bottom. The right panel's boundary corresponds to the black box's boundary on the left panel.

blocking fracture do so by taking the harmonic average of the transmissivity. This assumption differs from the AEM model, described in Toller (2022). In the AEM model, the draining and blocking fractures are treated separately instead of taking the harmonic average for the intersection.

A modified version of the AEM model was developed to replicate better the intersection behavior of the models presented in Flemisch et al. (2018). In this modified model, a small segment with lower transmissivity replaces part of the draining fracture before the intersection with a block fracture. The solutions are presented in Figure 9.5 and 9.6. This AEM model and the reference solution are almost identical, with a mean difference of 0.32% (flow left to right) and 0.14% (flow top to bottom); the difference between the AEM model and the reference solution is negligible. The most significant difference is now at the fracture tip of a draining fracture, which might be due to the large gradient there.

An issue when comparing the reference solution to the AEM model and the other methods is that the reference solution is also an FDM model, even though with high precision. A more accurate comparison would be to compare to an exact solution where the result is precisely determined. Such a comparison is, however, not possible for such complex fracture networks as no exact solutions are available.

This comparison shows that it is possible to get almost the same result with an AEM model as an FDM with a very high resolution. A benefit of the AEM

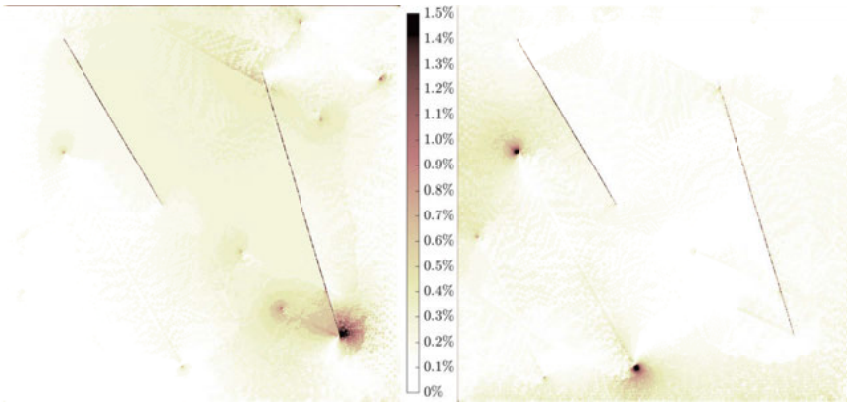

Figure 9.6. Contour of hydraulic head difference, $\Delta\tilde{\phi}$, between reference solution and the modified AEM model for flow left to right (left) and flow top to bottom (right).

model is that it is fast. As a reference, the AEM model took 15 seconds[1] to solve the simulation and 35 seconds to plot the flow net and the hydraulic head contour on a 400×400 grid. The time it takes to plot the solution linearly depends on the number of grid points used for the contour. The model is parallelized, which reduces computational time on processors with multiple cores. The solution and the resolution of the plot are independent of each other.

This comparison demonstrates that the AEM is an excellent benchmarking tool that efficiently gives a precise solution. Because the resolution of the flow net and hydraulic head contours are independent of the accuracy of the solution, the user can reiterate many models for calibration before producing high-resolution plots.

[1]On a HP Z2 Tower G4 Workstation with 32 GB RAM and an Intel(R) Core(TM) i7-9700K CPU @ 3.60GHz, 3600 Mhz, 8 cores, 8 logical processors

Part IV:
Summary and Conclusions

10. Discussion

This work has developed several AEM models for fractured rocks dealing with groundwater flow, linear elasticity, and a combination of the two. The benefits of these models are that they are both very accurate, up to machine precision, and computationally effective.

In summary, major contributions are in the form of four new analytic element models, which are:

- an analytic element model that incorporates the fractures properties in a continuum as a vertically varying hydraulic conductivity,
- an analytic element model for intersecting and heterogeneous fractures in groundwater flow,
- an analytic element model for intersecting fractures in a linearly elastic plane strain medium, and
- an analytic element model that includes seepage forces in a linearly elastic plane strain medium.

The most important benefits of these analytic element models are that they:

- are written in terms of analytic solutions,
- have no theoretical limitation on the number of elements in a model,
- give machine precision accuracy at every point in the domain, and
- are computationally efficient.

The papers presented in this thesis model a fractured rock using AEM for groundwater flow and linear elasticity. There are closed-form solutions for both of these cases. They are, however, limited to elementary and predetermined geometries, limiting the capabilities of these models. The AEM model developed here allows for a more flexible geometry while providing solutions up to machine precision. This means that the entire fractured rock mass can be modeled with the same model, from the regional to local scale. This is demonstrated by modeling all the different scales presented in Figure 1.2 as a linearly elastic medium in Figure 7.1 and 7.2. The model is also very fast, as demonstrated in the benchmarking example, where it only took the AEM model 50 seconds to solve the problem and plot the results with an averaged difference of 0.32% and 0.14% compared to the reference solution.

Papers I and II give two new ways of modeling the groundwater flow in fractured rocks. Paper I includes the fracture properties in a continuum, while Paper II allows for a discrete representation of the fractures. The continuum representation is better suited for more regional models, while a discrete representation is preferable on the local scale. In comparison, previous analytic models are limited to simple geometries, e.g., (Kitterød, 2004), (Şen, 1989)

and (Şen, 2014), the presented model includes interface flow, wells, lakes, and recharge, which further expand the applicability. Papers I and II provide groundwater flow analysis models for precisely representing flow near singular points, such as wells, with machine precision and an accurate path line determination. This also applies to the intersections of fractures where previous analytic element models, e.g., (Strack, 1982) and (Steward, 2015), cannot handle intersections without approximations.

Paper III provides the first large-scale model for AEM in linearly elastic media. The possibility of a theoretically unlimited number of fractures combined with the analytic representation of the tips is valuable. As demonstrated, it is possible to model the combined effect from 10,000 fractures and to determine the variables at every point in the domain. This property helps to validate numerical models and model laboratory experiments where a high degree of accuracy is required. Although analytic models exist for fractured media, e.g., (Chudnovsky and Kachanov, 1983), (Hori and Nemat-Nasser, 1987) and (Helsing, 2000), they do not possess the same number of degrees of freedom as the proposed model. As in Paper IV, the analytic element for a fracture presented in this thesis may also be combined with other analytic elements, e.g., tunnels, further extending its applicability.

Paper IV summarizes the findings by combining the groundwater flow with the linearly elastic model. By including the seepage force as a body force, the effect of seepage can be modeled near singular points. Determining the seepage effect at a fracture tip is difficult as stresses go to infinity. The AEM model in Paper IV makes the modeling of these points possible. Although seepage forces often are neglected when gravity is considered, knowing when this assumption is possible is essential. Paper IV provides the necessary functions to determine this. Unlike Park et al. (2008), this analytic method models fractures and tunnels and provides a more flexible tool to investigate seepage forces in fractured rocks.

One of the significant disadvantages of AEM is that it is not well suited for highly heterogeneous domains, where the medium varies significantly locally. Because AEM is meshless and constructed with elements, each heterogeneity must use at least one element. This property is unlike in meshed models, not naturally embedded in the models but will require the addition of many elements. In contrast, a meshed model already has a mesh of cells that can individually assign parameters.

Naturally, the construction and assumptions limit analytic element models. The geometry must be simplified to represent the solution using an analytic function. Although line elements can create any polygon, the number of elements will increase the computational time. Generally, AEM models are high-speed, and speed is seldom an issue. However, limiting the number of elements is always better for speed and control. For fractured rocks, AEM provides a valuable screening tool; even though it has some simplification, it provides a fast, accurate, and quick set-up model.

11. Outlook

Another natural next step would be to create a hydro-mechanical coupling that enables the linearly elastic model to impact groundwater flow or even one that functions in both directions through an iterative process. This coupling could be achieved by developing a function that links the aperture of a fracture to the stress state. This relationship has been extensively studied, e.g., (Malama and Kulatilake, 2003), (Bandis et al., 1983) and (Barton et al., 1985), and an empirical formula that translates the normal stress to a deformation in the fracture aperture is relatively straightforward to implement.

Another potential advancement in developing AEM for fractured rocks is to expand the fracture flow to three dimensions. The fundamentals already exist, where a circular or elliptical enclosing analytic element, (Ausk, 2018), can create an impermeable boundary. The solution is almost identical to that in Ausk (2018); the only difference is that the Cauchy integral is changed to produce the coefficients for a constant stream function boundary instead of a constant equipotential.

What remains is the development of an analytic element for the intersection of these three-dimensional fractures. If each fracture is considered a fully defined system, the flow between fractures would only discharge through an analytic element for intersections. Figure 11.1 presents two intersecting fractures with an inflow from a point source in one and an outflow in a line element in the other.

A great benefit of a three-dimensional analytic element model for fractures is that a superblock approach is built-in to the formulation. Superblocks are very useful for computational speed, as demonstrated in Craig et al. (2006). Because each fracture is connected to the intersection once via an intersection element, the effect from all other fractures also comes through that intersection element. Thus, the element solved for will get the combined effect from all fractures while only considering the fractures with shared intersections. The superblock combined with an efficient and parallelized scheme, e.g., in FORTRAN or C++, provides a fast and accurate model.

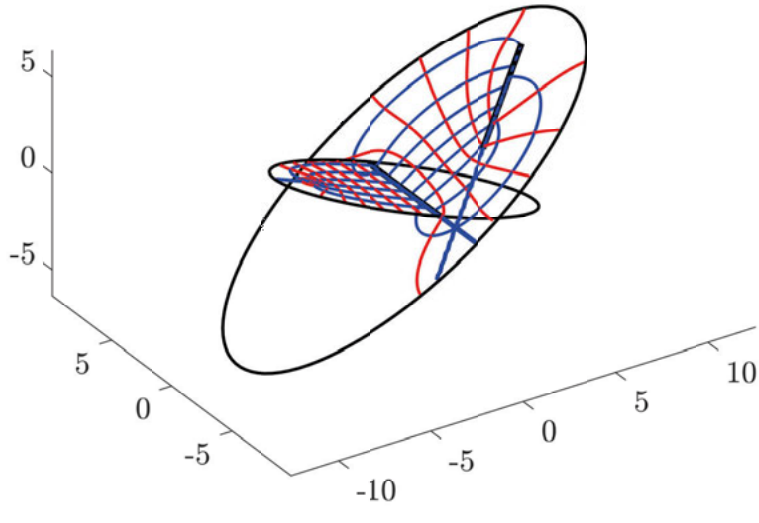

Figure 11.1. Two intersecting elliptical fractures in a three-dimensional space.

12. Acknowledgement

First, I would like to thank my principal supervisor, Auli Niemi. Without you, it wouldn't have been possible to do this. You have shown me what it means to be a researcher and how to succeed. I am grateful that you welcomed me to Uppsala and encouraged me to follow my ambitions.

I sincerely thank Otto Strack, my co-supervisor and co-author. Working with you has been a great pleasure, and you have helped me grow as a researcher. This thesis was only possible with your help. I am grateful for all of our discussions and debates. I would also like to thank Andrine Strack for always welcoming me to the farm and for your kindness.

I am grateful for the invaluable assistance of my co-supervisors, Qinghua Lei and Alexandru Tatomir. I truly enjoyed my enlightening discussions on fracture modeling with Qinghua and our shared research interests. Alexandru Tatomir, my former co-supervisor, guided me on the numerical modeling of fracture networks. Their contributions were instrumental in the success of my project.

I would also like to thank my colleagues at LUVAL for the encouraging atmosphere and working environment. A special thanks to all of my roommates that I have had throughout the years. Ramin, you have truly understood the struggles of a Ph.D. and gave me great help in getting through the process. Thank you to all my other roommates, Linus, Rohan, and Jai, who allowed me to talk about something else for a while.

I am also very thankful for my superiors at Trafikverket, Josef Malas and Havin Nyqvist, who helped fund the Ph.D. and have always been supportive.

Many thanks to the members of my reference group, Caroline Karlsson, Klas Hansson, and Jonas Sundell, for all our discussion and your input. You have helped me relate my work to reality and encouraged me along the way.

I would also like to thank my friends Peter Dirks and Anna Solfest for keeping me company while I was in the US during my travels. Getting company and a place to sleep in exchange for a bag of Swedish candy is a fair deal.

I am also grateful for the support of my mum, Anna, and dad, Björn, and their enthusiasm to see me succeed. Furthermore, I want to thank my brother and sister, Carl and Lisa, for being there when I felt like complaining about the many problems when doing a Ph.D.

I dedicate this thesis to my wife, Julia, and my children, Edith and Ture. Julia, you have always been by my side, and even though you have little clue about what I do, you support me. Edith, you always put a smile on my face and share my interest in rocks. Ture, you have taught me that the most important things in life are found at home.

The project was funded by Trafikverket under Grant No. 7017, and I am truly grateful for this opportunity. Sharing my time between Trafikverket and Uppsala University has given me the best of two worlds.

13. Sammanfattning på svenska

Det finns ett stort behov och intresse av att använda berg som en potentiell plats för viktiga framtida investeringar, såsom byggandet av infrastruktur, lagring av kärnavfall, energiutvinning och gruvdrift. För att projekt i berg ska vara kostnadseffektiva och säkra måste bergets egenskaper karakteriseras samt dess påverkan på grundvattnet och det mekaniska tillståndet undersökas. Att fånga bergets egenskaper är svårt, i synnerhet eftersom berget typiskt är mycket heterogent och kännetecknas av olika attribut. Dessa attribut kan till exempel utgöra sprickor, sprickzoner, tunnlar, bergrum och brunnar som alla påverkar grundvattenflödet och mekaniken i olika omfattning. Sambanden mellan dem är komplexa och kan därmed vara svåranalyserade.

Nyttjandet av berg spelar en avgörande roll i övergången till en mer hållbar miljö och för att mildra klimatförändringarna. Genom att flytta transporter och infrastruktur under jord frigörs istället utrymme ovan jord, vilket ökar förutsättningarna för att nå de globala hållbarhetsmålen, till exempel hållbart nyttjande av ekosystemen och ökad biologisk mångfald. Dessutom kan berget användas för energiproduktion. Enligt Goldstein et al. (2011) är energibrunnar redan en betydande bidragsgivare till fossilfri el- och energiproduktion. I Sverige finns för närvarande över 300 000 energibrunnar (Svergie Geologiska Undersökning, 2023) och ett ständigt växande behov. För att kunna tillgodose det växande behovet är det viktigt att kartlägga hur de påverkar varandra och hur de påverkas av andra anläggningar.

Förutom brunnar för energiproduktion är även brunnar för dricksvattenförsörjning viktiga och enligt Livsmedelsverket (2023) använder idag över en miljon svenskar privata brunnar för sin dricksvattenförsörjning. Dessa brunnar riskerar att påverkas av både klimatförändringar och byggprojekt. Därför är det betydelsefullt att övervaka brunnarnas kvalitet och kapacitet, framförallt i känsliga miljöer med ont om grundvatten såsom öar. Det finns även ett behov av att kartlägga hur befintliga och planerade byggprojekt kan påverka eller skada dagens och framtidens dricksvattenförsörjning.

För att förstå hur grundvatten och berg påverkas av befintliga och planerade byggprojekt är det avgörande att berget studeras och dess egenskaper karakteriseras. I Sverige är det vanligt med sprickigt kristallint berg som har distinkta egenskaper i både den intakta bergmassan och sprickorna. Den intakta bergmassan har en mycket låg permeabilitet och är relativt homogen. Sprickorna fungerar å andra sidan som den primära vägen för grundvattentransport och diskontinuiteter i spännings- och deformationstillståndet. Modellerna som används för att studera dessa bergarter måste således på lämpligt sätt beakta

förekomsten av sprickor. En utmaning är att merparten av informationen om berget och dess sprickor hämtas från borrhål som endast representerar en liten del av den totala bergmassan. Det är då hjälpsamt med en modell som effektivt kan simulera många olika uppsättningar med tänkbara egenskaper och ge ett spektrum av möjliga utfall.

Huvudsyftet med denna avhandling är att utveckla analytiska elementmodeller för att simulera sprickigt berg som ett linjärt elastiskt material och studera grundvattenflödet genom det. Fokus ligger på att matematiskt noggrant hantera sprickorna genom att formulera dem i termer av så kallade analytiska element. Dessutom kombineras bergmekaniska processer och grundvattenflödet genom att inkludera strömningskraften från grundvattnet i den mekaniska, linjära och elastiska modellen.

Den analytiska elementmetoden (Analytic Element Method, AEM) utgör grunden för att utveckla dessa modeller. AEM introducerades ursprungligen av Strack (1989) under 80-talet. Den kombinerar en uppsättning analytiska lösningar för att bygga modeller med hög precision. Dessa modeller har flera fördelar, vilka bland annat är att de:

- är skrivna i termer av analytiska lösningar,
- har ingen teoretisk begräsning i sin storlek eller detaljrikedom,
- genererar lösningar med maskinprecision, och
- är beräkningseffektiva.

Metoden är dock inte lämplig för att modellera mycket heterogena ytor eftersom det kräver att en stor mängd analytiska element används. Tekniken är inte heller lika välutvecklad eller kommersiellt tillgänglig som andra numeriska modeller.

Vid modellering av sprickor i berg finns tre alternativ: att behandla dem som ett kontinuum, som diskreta sprickor eller som en kombination av de två. **Artikel I** i denna avhandling introducerar en modell som inkluderar sprickorna som ett kontinuum, med hjälp av en hydraulisk konduktivitet som varierar med djupet för att bättre representera sprickornas egenskaper. Den hydrauliska konduktiviteten varierar fritt med djupet. Som exempel presenteras en modell över en ö där saltvatteninträngning i brunnar övervakas. Modellen kan snabbt och noggrant beräkna villkoren för pumpkapacitet till en uppsättning brunnar på ön. Trots sin enkelhet inkluderar modellen effekterna av vertikal variation av hydraulisk konduktivitet, vilket gör den användbar för flöden i sprickigt berg, där variationen i hydraulisk konduktivitet med djupet är betydande.

Den andra artikeln, **Artikel II**, presenterar en modell för grundvattenflöde i diskreta sprickor inom ett kontinuum. Modeller för både flödesblockerande och dränerande sprickor utvecklas. Genom att modellera korsande sprickor med flera element som möts i skärningspunkten behövs inga approximationer, vilket gör metodiken exakt. Samma metodik kan användas för att modellera heterogenitet i enskilda sprickors transmissivitet genom att modellera en spricka med flera sammansatta element. Randvillkoren för dessa element är att kontinuitet i grundvattennivå och flöde uppfylls längs hela sprickan samt

vid alla mötespunkter mellan elementen. Artikeln visar bland annat hur en ensemble av sprickor med olika transmissivitet påverkar grundvattenflödet runt en tunnel.

Artikel III beskriver den första modellen for linjär elasticitet inom AEM. Linjär elasticitet beskriver hur berget deformeras på grund av spänningsförhållanden. Denna modell bygger på att varje spricka representeras av ett analytiskt element. Dessa element tillåts att korsa varandra. Randvillkoren är formulerade i termer av spänningsvektorer och det analytiska elementet uttrycks i form av en asymptotisk serie. En simulering konstruerades med 10 000 sprickor i ett uniformt spänningsfält. I modellen påverkas varje enskild spricka av bidraget från alla andra sprickor. Lösningen har samma precision i både den större skalan, som tar till hänsyn alla sprickor i domänen, och den mindre skalan, där närområdet för enskilda sprickor studeras.

I **Artikel IV** kombineras grundvatten och linjärelasticitet genom att grundvattenflödet ingår som en strömningskraft i den linjärelastiska modellen. Både strömningskrafterna och gravitationen är integrerade i den linjära elastiska lösningen. Artikeln presenterar lösningen för både sprickor och tunnlar. Kopplingen mellan grundvattenmodellen och den linjära elastiska modellen är enkelriktad på det sättet att grundvattenmodellen påverkar spänningstillståndet men antas vara oförändrad av det. Modellen visar att strömningskrafterna blir högre med djupet och att om det finns ett artesiskt tryck kan strömningskrafterna överstiga krafterna från gravitationen.

I slutet av avhandlingen genomförs en jämförelsestudie mellan en av de utvecklade modellerna och en tidigare studie (Flemisch et al., 2018) med en uppsättning av flera befintliga numeriska modeller. Resultaten visar att AEM-modellen är kapabel att generera en lösning med en felmarginal på mindre än en halv procent jämfört med referenslösningen från den tidigare studien. Detta är bättre än alla de andra numeriska modeller som presenterades i studien. Resultaten motiverar att använda AEM-modellen som en benchmarking-modell. AEM-modellen är förutom att vara snabb också giltig i olika skalor, vilket skapar möjligheter inom dess tillämpningsområden.

Sammanfattningsvis fokuserar denna avhandling på modellering av grundvattenflödet och linjär elasticitet i sprickigt berg med hjälp av AEM. Två modeller har utvecklats för grundvattenflödet, varav den ena behandlar sprickor genom att summera dess djupberoende egenskaper i ett kontinuum och den andra behandlar diskreta sprickor i ett kontinuum. Dessutom har två modeller för linjär elasticitet utvecklats, varav den ena beskriver diskreta sprickor i en bergmassa och den andra beskriver sprickor och tunnlar i en bergmassa utsatt för strömningskrafter och gravitation. Alla dessa modeller bidrar till att öka förståelsen för hur sprickigt berg beter sig med avseende på grundvattenflöde och bergmekanik. Eftersom de är formulerade som analytiska funktioner begränsas resultatet endast av maskinprecisionen, vilket gör att resultatet är exakt och kan till exempel simulera förhållanden med extrema gradienter. Dessa egenskaper är användbara för att till exempel validera numeriska model-

ler. Modellerna är även beräkningseffektiva och kan snabbt simulera problem, vilket är fördelaktigt i olika typer av förstudier.

References

Anagnostou, G. and Kovári, K. (1996). Face stability conditions with earth-pressure-balanced shields. *Tunnelling and underground space technology*, 11(2):165–173.

Arbogast, T., Cowsar, L. C., Wheeler, M. F., and Yotov, I. (2000). Mixed finite element methods on nonmatching multiblock grids. *SIAM Journal on Numerical Analysis*, 37(4):1295–1315.

Ausk, B. K. (2018). *An Enclosing Analytic Element*. PhD thesis, University of Minnesota.

Bakker, M. (2004). Transient analytic elements for periodic dupuit–forchheimer flow. *Advances in Water Resources*, 27(1):3–12.

Bakker, M., Anderson, E. I., Olsthoorn, T., and Strack, O. D. L. (1999). Regional groundwater modeling of the yucca mountain site using analytic elements. *Journal of Hydrology*, 226(3-4):167–178.

Bandis, S., Lumsden, A., and Barton, N. (1983). Fundamentals of rock joint deformation. In *International Journal of Rock Mechanics and Mining Sciences & Geomechanics Abstracts*, volume 20, pages 249–268. Elsevier.

Banks-Sills, L. (1991). Application of the finite element method to linear elastic fracture mechanics. *Applied Mechanics Reviews*.

Barnes, R. and Janković, I. (1999). Two-dimensional flow through large numbers of circular inhomogeneities. *Journal of Hydrology*, 226(3-4):204–210.

Barton, N., Bandis, S., and Bakhtar, K. (1985). Strength, deformation and conductivity coupling of rock joints. In *International journal of rock mechanics and mining sciences & geomechanics abstracts*, volume 22, pages 121–140. Elsevier.

Benthem, J. and Koiter, W. (1973). Asymptotic approximations to crack problems. *Methods of analysis and solutions of crack problems: Recent developments in fracture mechanics Theory and methods of solving crack problems*, pages 131–178.

Benveniste, Y., Dvorak, G., Zarzour, J., and Wung, E. (1989). On interacting cracks and complex crack configurations in linear elastic media. *International Journal of Solids and Structures*, 25(11):1279–1293.

Berkowitz, B. (2002). Characterizing flow and transport in fractured geological media: A review. *Advances in Water Resources*, 25(8-12):861–884.

Berre, I., Boon, W. M., Flemisch, B., Fumagalli, A., Gläser, D., Keilegavlen, E., Scotti, A., Stefansson, I., Tatomir, A., Brenner, K., et al. (2021). Verification benchmarks for single-phase flow in three-dimensional fractured porous media. *Advances in Water Resources*, 147:103759.

Berzell, A. (2011). *E4 Förbifart Stockholm - PM Hydrogeologi*. Trafikverket. Tillståndsansökan Miljöbalken - 0G14H032.

Bonnet, E., Bour, O., Odling, N. E., Davy, P., Main, I., Cowie, P., and Berkowitz, B. (2001). Scaling of fracture systems in geological media. *Reviews of geophysics*, 39(3):347–383.

Boon, W. M., Nordbotten, J. M., and Yotov, I. (2018). Robust discretization of flow in fractured porous media. *SIAM Journal on Numerical Analysis*, 56(4):2203–2233.
Bour, O. and Davy, P. (1997). Connectivity of random fault networks following a power law fault length distribution. *Water Resources Research*, 33(7):1567–1583.
Bour, O. and Davy, P. (1998). On the connectivity of three-dimensional fault networks. *Water Resources Research*, 34(10):2611–2622.
Brezzi, F., Lipnikov, K., and Simoncini, V. (2005). A family of mimetic finite difference methods on polygonal and polyhedral meshes. *Mathematical Models and Methods in Applied Sciences*, 15(10):1533–1551.
Carlsson, A. and Olsson, T. (1977). Hydraulic properties of swedish crystalline rocks. *Bulletin of the Geological Institute, University of Uppsala, NS*, 7:71–84.
Charny, I. A. (1951). A rigorous derivation of dupuit's formula for unconfined seepage with seepage surface. *Doklady Akademii Nauk, Moscow*, 79(6).
Chudnovsky, A., Dolgopolsky, A., and Kachanov, M. (1987). Elastic interaction of a crack with a microcrack array-i. formulation of the problem and general form of the solution. *International Journal of Solids and Structures*, 23(1):1–10.
Chudnovsky, A. and Kachanov, M. (1983). Interaction of a crack with a field of microcracks. *International Journal of Engineering Science*, 21(8):1009–1018.
Craig, J. R., Janković, I., and Barnes, R. (2006). The nested superblock approach for regional-scale analytic element models. *Groundwater*, 44(1):76–80.
Craig, J. R. and Read, W. W. (2010). The future of analytical solution methods for groundwater flow and transport simulation. In *Computational Methods in Water Resources (CMWR)*, Barcelona, Spain.
D'Angelo, C. and Scotti, A. (2012). A mixed finite element method for darcy flow in fractured porous media with non-matching grids. *ESAIM: Mathematical Modelling and Numerical Analysis-Modélisation Mathématique et Analyse Numérique*, 46(2):465–489.
De Lange, W. (1996). Nagrom, a model for national groundwater management and regional and local studies. *European Water Pollution Control*, 5(6):63–67.
De Lange, W. (2006). Development of an analytic element ground water model of the netherlands. *Groundwater*, 44(1):111–115.
De Marsily, G. (1986). Quantitative hydrogeology. Technical report, Paris School of Mines, Fontainebleau.
Dupuit, J. (1863). *Études théoretiques et pratiques sur le mouvement des eaux dans les canaux découverts et à travers les terrains perméables*. Dunod, Paris.
Ericsson, L. O. and Ronge, B. (1986). Correlation between tectonic lineaments and permeability values of crystalline bedrock in the gideå area. Technical report, Swedish Nuclear Fuel and Waste Management Co.
Fang, Q., Song, H., and Zhang, D. (2015). Complex variable analysis for stress distribution of an underwater tunnel in an elastic half plane. *International Journal for Numerical and Analytical Methods in Geomechanics*, 39(16):1821–1835.
Figueiredo, B., Tsang, C.-F., Rutqvist, J., and Niemi, A. (2015). A study of changes in deep fractured rock permeability due to coupled hydro-mechanical effects. *International Journal of Rock Mechanics and Mining Sciences*, 79:70–85.
Fiori, A., Janković, I., and Dagan, G. (2006). Modeling flow and transport in highly heterogeneous three-dimensional aquifers: Ergodicity, gaussianity, and anomalous behavior - 2. approximate semianalytical solution. *Water Resources Research*,

42(6).
Fitts, C. R. (1989). Simple analytic functions for modeling three-dimensional flow in layered aquifers. *Water Resources Research*, 25(5):943–948.
Flemisch, B., Berre, I., Boon, W., Fumagalli, A., Schwenck, N., Scotti, A., Stefansson, I., and Tatomir, A. (2018). Benchmarks for single-phase flow in fractured porous media. *Advances in Water Resources*, 111:239–258.
Flemisch, B. and Rainer, H. (2008). Numerical investigation of a mimetic finite difference method. *Finite volumes for complex applications V–Problems and perspectives*, pages 815–824.
Forchheimer, P. (1886). Über die ergiebigkeit von brunnen-anlagen und sickerschlitzen. zd achitektenu. ing. *Verein*, 32:539–564.
Fu, J., Yang, J., Yan, L., and Abbas, S. M. (2015). An analytical solution for deforming twin-parallel tunnels in an elastic half plane. *International Journal for Numerical and Analytical Methods in Geomechanics*, 39(5):524–538.
Fu, P., Johnson, S. M., and Carrigan, C. R. (2013). An explicitly coupled hydro-geomechanical model for simulating hydraulic fracturing in arbitrary discrete fracture networks. *International Journal for Numerical and Analytical Methods in Geomechanics*, 37(14):2278–2300.
Gerolymatou, E. (2019). A novel tool for simulating brittle borehole breakouts. *Computers and Geotechnics*, 107:80–88.
Goldstein, B., Hiriart, G., Bertani, R., Bromley, C., and Gutiérrez-Negrín, L. (2011). Geothermal energy. *Renewable Energy Sources and Climate Change Mitigation. Special report of the intergovernmental panel on climate change.*, 106:401–436.
Goodman, R., Moye, D., Van Schalkwyk, A., and Javandel, I. (1964). *Ground Water Inflows During Tunnel Driving*. College of Engineering, University of California.
Griffith, A. A. (1921). The phenomena of rupture and flow in solids. *Philosophical transactions of the royal society of london. Series A, containing papers of a mathematical or physical character*, 221(582-593):163–198.
Gustafson, G. (2009). *Hydrogeologi för bergbyggare*, volume 2009:2. Formas, Stockholm.
Hadgu, T., Karra, S., Kalinina, E., Makedonska, N., Hyman, J. D., Klise, K., Viswanathan, H. S., and Wang, Y. (2017). A comparative study of discrete fracture network and equivalent continuum models for simulating flow and transport in the far field of a hypothetical nuclear waste repository in crystalline host rock. *Journal of Hydrology*, 553:59–70.
Haitjema, H. M. (1985). Modeling three-dimensional flow in confined aquifers by superposition of both two-and three-dimensional analytic functions. *Water Resources Research*, 21(10):1557–1566.
Haitjema, H. M. (1995). *Analytic element modeling of groundwater flow*. Elsevier.
Haitjema, H. M. and Strack, O. D. L. (1985). An initial study of thermal energy storage in unconfined aquifers. *Final report to Battelle Pacific-Northwest laboratory*.
Harrison, J. P., Hudson, J. A., and Popescu, M. (2002). Engineering rock mechanics: Part 2. illustrative worked examples. *Applied Mechanics Reviews*, 55(2):B30–B31.
He, X., Sinan, M., Kwak, H., and Hoteit, H. (2021). A corrected cubic law for single-phase laminar flow through rough-walled fractures. *Advances in Water Resources*, 154:103984.

Heister, T., Rebholz, L. G., and Xue, F. (2019). *Numerical analysis: an introduction*. De Gruyter, Berlin;Boston;.

Helsing, J. (2000). Fast and accurate numerical solution to an elastostatic problem involving ten thousand randomly oriented cracks. *International Journal of Fracture*, 100:321–327.

Hoek, E. and Brown, E. T. (1997). Practical estimates of rock mass strength. *International journal of rock mechanics and mining sciences*, 34(8):1165–1186.

Hori, M. and Nemat-Nasser, S. (1987). Interacting micro-cracks near the tip in the process zone of a macro-crack. *Journal of the Mechanics and Physics of Solids*, 35(5):601–629.

Horii, H. and Nemat-Nasser, S. (1985). Elastic fields of interacting inhomogeneities. *International Journal of Solids and Structures*, 21(7):731–745.

Huang, N., Liu, R., Jiang, Y., and Cheng, Y. (2021). Development and application of three-dimensional discrete fracture network modeling approach for fluid flow in fractured rock masses. *Journal of Natural Gas Science and Engineering*, 91:103957.

Inglis, C. E. (1913). Stresses in a plate due to the presence of cracks and sharp corners. *Transactions of the Institution of Naval Architectures*, 55:219–241.

Irwin, G. R. (1957). Analysis of stresses and strains near the end of a crack traversing a plate. *Journal of Applied Mechanics*, 24:361–364.

Ivars, D. M. (2006). Water inflow into excavations in fractured rock – a three-dimensional hydro-mechanical numerical study. *International Journal of Rock Mechanics and Mining Sciences*, 43(5):705–725.

Jankovic, I., Fiori, A., and Dagan, G. (2006). Modeling flow and transport in highly heterogeneous three-dimensional aquifers: Ergodicity, gaussianity, and anomalous behavior - 1. conceptual issues and numerical simulations. *Water Resources Research*, 42(6):W06D12.

Jing, L. (2003). A review of techniques, advances and outstanding issues in numerical modelling for rock mechanics and rock engineering. *International Journal of Rock Mechanics and Mining Sciences*, 40(3):283–353.

Jing, L. and Hudson, J. (2002). Numerical methods in rock mechanics. *International Journal of Rock Mechanics and Mining Sciences*, 39(4):409–427.

Kachanov, M. (1993). Elastic solids with many cracks and related problems. *Advances in applied mechanics*, 30:259–445.

Karimi-Fard, M., Durlofsky, L. J., and Aziz, K. (2004). An efficient discrete-fracture model applicable for general-purpose reservoir simulators. *SPE journal*, 9(02):227–236.

Khanal, A. and Weijermars, R. (2019). Modeling flow and pressure fields in porous media with high conductivity flow channels and smart placement of branch cuts for variant and invariant complex potentials. *Fluids*, 4(3):154.

Khanal, A. and Weijermars, R. (2020). Comparison of flow solutions for naturally fractured reservoirs using complex analysis methods (cam) and embedded discrete fracture models (edfm): Fundamental design differences and improved scaling method. *Geofluids*, 2020.

Kitterød, N.-O. (2004). Dupuit-forchheimer solutions for radial flow with linearly varying hydraulic conductivity or thickness of aquifer. *Water Resources Research*, 40(11).

Kraemer, S. R. (1990). *Modeling of regional groundwater flow in fractured rock aquifers*. Indiana University.

Kraemer, S. R. (2007). Analytic element ground water modeling as a research program (1980 to 2006). *Groundwater*, 45(4):402–408.

Kuna, M. (2013). *Finite Elements in Fracture Mechanics: Theory-Numerics-Applications*, volume 201. Springer Science & Business Media.

Kusumoto, S. and Gudmundsson, A. (2014). Displacement and stress fields around rock fractures opened by irregular overpressure variations. *Frontiers in Earth Science*, 2(May).

Kusumoto, S., Gudmundsson, A., Simmenes, T. H., Geshi, N., and Philipp, S. L. (2013). Inverse modeling for estimating fluid-overpressure distributions and stress intensity factors from an arbitrary open-fracture geometry. *Journal of Structural Geology*, 46:92–98.

Lee, I.-M. and Nam, S.-W. (2001). The study of seepage forces acting on the tunnel lining and tunnel face in shallow tunnels. *Tunnelling and Underground Space Technology*, 16(1):31–40.

Lei, Q., Latham, J.-P., and Tsang, C.-F. (2017). The use of discrete fracture networks for modelling coupled geomechanical and hydrological behaviour of fractured rocks. *Computers and Geotechnics*, 85:151–176.

Lei, Q. and Wang, X. (2016). Tectonic interpretation of the connectivity of a multiscale fracture system in limestone. *Geophysical Research Letters*, 43(4):1551–1558.

Leitman, M. J. and Villaggio, P. (2005). An extension of the complex variable method in plane elasticity to domains with corners: A notch problem. *Journal of Elasticity*, 81(2):205–215.

LeVeque, R. J. (2007). *Finite difference methods for ordinary and partial differential equations: steady-state and time-dependent problems*. Society for Industrial and Applied Mathematics, Philadelphia, PA.

Lissel, P. (2016). *PM Hydrogeologiska beräkningar - Bilaga 2 PM Numerisk grundvattenberäkning Haga, Korsvägen och Almedal*. Trafikverket. TRV 2016/3151 - MPU02-50GT-025-00-0006_Bilaga 2.

Liu, G. R. and Quek, S. S. (2003). *The finite element method: a practical course*. Butterworth-Heinemann, Oxford;Boston;.

Livsmedelsverket (2023). Egen brunn eller annan liten dricksvattenanläggning för privat bruk. `https://www.livsmedelsverket.se/livsmedel-och-innehall/dricksvatten/egen-brunn2`. Published: 2022-10-10.

Long, J. C., Remer, J., Wilson, C., and Witherspoon, P. (1982). Porous media equivalents for networks of discontinuous fractures. *Water Resources Research*, 18(3):645–658.

Malama, B. and Kulatilake, P. (2003). Models for normal fracture deformation under compressive loading. *International Journal of Rock Mechanics and Mining Sciences*, 40(6):893–901.

Mazumder, S. (2015). *Numerical methods for partial differential equations: finite difference and finite volume methods*. Academic Press.

Min, K.-B., Jing, L., and Stephansson, O. (2004a). Determining the equivalent permeability tensor for fractured rock masses using a stochastic rev approach:

method and application to the field data from sellafield, uk. *Hydrogeology Journal*, 12:497–510.

Min, K.-B., Rutqvist, J., Tsang, C.-F., and Jing, L. (2004b). Stress-dependent permeability of fractured rock masses: a numerical study. *International Journal of Rock Mechanics and Mining Sciences*, 41(7):1191–1210.

Minkoff, S. E., Stone, C. M., Bryant, S., Peszynska, M., and Wheeler, M. F. (2003). Coupled fluid flow and geomechanical deformation modeling. *Journal of Petroleum Science and Engineering*, 38(1-2):37–56.

Mohammadnejad, M., Liu, H., Chan, A., Dehkhoda, S., and Fukuda, D. (2021). An overview on advances in computational fracture mechanics of rock. *Geosystem Engineering*, 24(4):206–229.

Muskhelishvili, N. I. (1953). *Some basic problems of the mathematical theory of elasticity*, volume 15. Noordhoff Groningen.

Neuman, S. P. (1987). Stochastic continuum representation of fractured rock permeability as an alternative to the rev and fracture network concepts. In *ARMA US Rock Mechanics/Geomechanics Symposium*, pages ARMA–87. ARMA.

Neuman, S. P. (2005). Trends, prospects and challenges in quantifying flow and transport through fractured rocks. *Hydrogeology Journal*, 13:124–147.

Niemi, A., Kontio, K., Kuusela-Lahtinen, A., and Poteri, A. (2000). Hydraulic characterization and upscaling of fracture networks based on multiple-scale well test data. *Water Resources Research*, 36(12):3481–3497.

Nordqvist, R., Gustafsson, E., Andersson, P., and Thur, P. (2008). Groundwater flow and hydraulic gradients in fractures and fracture zones at forsmark and oskarshamn. Technical Report SKB Rapport R-08-103, Svensk Kärnbränslehantering AB.

Oda, M. (1985). Permeability tensor for discontinuous rock masses. *Geotechnique*, 35(4):483–495.

Öhman, J. and Niemi, A. (2003). Upscaling of fracture hydraulics by means of an oriented correlated stochastic continuum model. *Water Resources Research*, 39(10).

Öhman, J., Niemi, A., and Tsang, C.-F. (2005a). Probabilistic estimation of fracture transmissivity from wellbore hydraulic data accounting for depth-dependent anisotropic rock stress. *International Journal of Rock Mechanics and Mining Sciences*, 42(5-6):793–804.

Öhman, J., Niemi, A., and Tsang, C.-F. (2005b). A regional-scale particle-tracking method for nonstationary fractured media. *Water Resources Research*, 41(3).

Omar, P. J., Gaur, S., Dwivedi, S., and Dikshit, P. (2019). Groundwater modelling using an analytic element method and finite difference method: an insight into lower ganga river basin. *Journal of Earth System Science*, 128:1–10.

Pan, Q. and Dias, D. (2018). Three dimensional face stability of a tunnel in weak rock masses subjected to seepage forces. *Tunnelling and Underground Space Technology*, 71:555–566.

Park, K.-H., Lee, J.-G., and Owatsiriwong, A. (2008). Seepage force in a drained circular tunnel: An analytical approach. *Canadian Geotechnical Journal*, 45(3):432–436.

Perazzelli, P., Leone, T., and Anagnostou, G. (2014). Tunnel face stability under seepage flow conditions. *Tunnelling and Underground Space Technology*,

43:459–469.
Perez, N. (2017). *Fracture Mechanics*. Springer International Publishing, Cham, 2nd ed. 2017. edition.
Reddy, J. N. (2019). *Introduction to the finite element method*. McGraw-Hill Education, New York.
Rice, J. R. et al. (1968). Mathematical analysis in the mechanics of fracture. *Fracture: an advanced treatise*, 2:191–311.
Rutqvist, J. and Stephansson, O. (2003). The role of hydromechanical coupling in fractured rock engineering. *Hydrogeology Journal*, 11:7–40.
Sadd, M. H. (2014). *Elasticity: theory, applications, and numerics*. Elsevier/AP, Amsterdam;Boston, third edition.
Şen, Z. (1989). Radial flow in vertically graded hydraulic conductivity aquifers. *Journal of Hydraulic Engineering*, 115(12):1667–1682.
Şen, Z. (2014). Hydraulic conductivity variation in a confined aquifer. *Journal of Hydrologic Engineering*, 19(3):654–658.
Sih, G. (1966). On the westergaard method of crack analysis. *International Journal of Fracture Mechanics*, 2:628–631.
Singh, B. (1973a). Continuum characterization of jointed rock masses: Part i-the constitutive equations. In *International Journal of Rock Mechanics and Mining Sciences & Geomechanics Abstracts*, volume 10, pages 311–335. Elsevier.
Singh, B. (1973b). Continuum characterization of jointed rock masses: Part ii-significance of low shear modulus. In *International Journal of Rock Mechanics and Mining Sciences & Geomechanics Abstracts*, volume 10, pages 337–349. Elsevier.
Sitharam, T., Sridevi, J., and Shimizu, N. (2001). Practical equivalent continuum characterization of jointed rock masses. *International Journal of Rock Mechanics and Mining Sciences*, 38(3):437–448.
Sneddon, I. (1973). Integral transform methods. *Methods of analysis and solutions of crack problems: Recent developments in fracture mechanics Theory and methods of solving crack problems*, pages 315–367.
Sneddon, I. and Elliot, H. (1946). The opening of a griffith crack under internal pressure. *Quarterly of Applied Mathematics*, 4(3):262–267.
Sneddon, I. N. (1946). The distribution of stress in the neighbourhood of a crack in an elastic solid. *Proceedings of the Royal Society of London. Series A. Mathematical and Physical Sciences*, 187(1009):229–260.
Snow, D. T. (1965). *A parallel plate model of fractured permeable media*. University of California, Berkeley.
Snow, D. T. (1969). Anisotropie permeability of fractured media. *Water Resources Research*, 5(6):1273–1289.
Steward, D. R. (2015). Analysis of discontinuities across thin inhomogeneities, groundwater/surface water interactions in river networks, and circulation about slender bodies using slit elements in the a nalytic e lement m ethod. *Water Resources Research*, 51(11):8684–8703.
Strack, O. and Haitjema, H. (1981a). Modeling double aquifer flow using a comprehensive potential and distributed singularities: 2. solution for inhomogeneous permeabilities. *Water Resources Research*, 17(5):1551–1560.

Strack, O. D. L. (1982). Assessment of effectiveness of geologic isolation systems. analytic modeling of flow in a permeable fissured medium. Technical report, Pacific Northwest Lab.

Strack, O. D. L. (1984). Three-dimensional streamlines in dupuit-forchheimer models. *Water Resources Research*, 20(7):812–822.

Strack, O. D. L. (1989). *Groundwater mechanics*. Prentice Hall.

Strack, O. D. L. (2003). Theory and applications of the analytic element method. *Reviews of Geophysics*, 41(2).

Strack, O. D. L. (2009). Using wirtinger calculus and holomorphic matching to obtain the discharge potential for an elliptical pond. *Water Resources Research*, 45(1).

Strack, O. D. L. (2017). *Analytical groundwater mechanics*. Cambridge University Press.

Strack, O. D. L. (2018). Limitless analytic elements. *Water Resources Research*, 54(2):1174–1190.

Strack, O. D. L. (2020). *Applications of vector analysis and complex variables in engineering*. Springer.

Strack, O. D. L. and Ausk, B. K. (2015). A formulation of groundwater flow in a stratified coastal aquifer using the dupuit-forchheimer approximation. *Water Resources Research*, 51:1–20.

Strack, O. D. L., Barnes, R. J., and Verruijt, A. (2006). Vertically integrated flows, discharge potential, and the dupuit-forchheimer approximation. *Groundwater*, 44(1):72–75.

Strack, O. D. L. and Haitjema, H. M. (1981b). Modeling double aquifer flow using a comprehensive potential and distributed singularities: 1. solution for homogeneous permeability. *Water Resources Research*, 17(5):1535–1549.

Strack, O. D. L. and Toller, E. A. L. (2022). An analytic element model for highly fractured elastic media. *International Journal for Numerical and Analytical Methods in Geomechanics*, 46(2):297–314.

Strack, O. E. and Verruijt, A. (2002). A complex variable solution for a deforming buoyant tunnel in a heavy elastic half-plane. *International Journal for Numerical and Analytical Methods in Geomechanics*, 26(12):1235–1252.

Svensson, H. and Lissel, P. (2017). *PM Hydrogeologi - Bilaga C6 Hydrogeologiska beräkningar Miljöprövning för tunnelbanan till Arenastaden*. Region Stockholm. FUT 2016-0025 - 3140-M35-22-01004_bilaga C6.

Svensson, H. and Lissel, P. (2019). *PM Hydrogeologi - Bilaga C6 Hydrogeologiska beräkningar Miljöprövning för utbyggd depå i Högdalen*. Region Stockholm. FUT 2016-0027 - 5140-M53-22-01003_bilaga C6.

Svergie Geologiska Undersökning (2023). Bergvärme. `https://www.sgu.se/samhallsplanering/energi/Geoenergi-geotermi-och-energilagring/bergvarme/`. Published: 2023-05-15.

Thomas, J. W. (2013). *Numerical partial differential equations: finite difference methods*, volume 22. Springer Science & Business Media, New York.

Toller, E. A. L. (2022). An analytic element model for intersecting and heterogeneous fractures in groundwater flow. *Water Resources Research*, 58(5):e2021WR031520.

Toller, E. A. L. and Strack, O. D. L. (2019). Interface flow with vertically varying hydraulic conductivity. *Water Resources Research*, 55(11):8514–8525.

Toller, E. A. L. and Strack, O. D. L. (2023). An analytic element model for seepage forces in fractured media. *International Journal for Numerical and Analytical Methods in Geomechanics (submitted)*, -(-):–.

Trafikverket (2023). Så sköter vi broar och tunnlar. `https://www.trafikverket.se/resa-och-trafik/underhall/sa-skoter-vi-broar-och-tunnlar/`. Published: 2023-02-03.

Tsang, C.-F. (1987). Introduction to coupled processes. *Coupled processes associated with nuclear waste repositories*, pages 1–5.

Tsang, C.-F., Figueiredo, B., and Niemi, A. (2018). Importance of stress effects on inputs to fracture network models used for subsurface flow and transport studies. *International Journal of Rock Mechanics and Mining Sciences*, 101:13–17.

van Harmelen, A. and Weijermars, R. (2018). Complex analytical solutions for flow in hydraulically fractured hydrocarbon reservoirs with and without natural fractures. *Applied Mathematical Modelling*, 56:137–157.

Verruijt, A. (1997). A complex variable solution for a deforming circular tunnel in an elastic half-space. *International Journal for Numerical and Analytical Methods in Geomechanics*, 21(2):77–89.

Wang, H. (2000). *Theory of linear poroelasticity with applications to geomechanics and hydrogeology*, volume 2. Princeton university press.

Weijermars, R. and Khanal, A. (2019). High-resolution streamline models of flow in fractured porous media using discrete fractures: Implications for upscaling of permeability anisotropy. *Earth-science reviews*, 194:399–448.

Weijermars, R., van Harmelen, A., and Zuo, L. (2016). Controlling flood displacement fronts using a parallel analytical streamline simulator. *Journal of Petroleum Science and Engineering*, 139:23–42.

Weijermars, R., van Harmelen, A., Zuo, L., Alves, I. N., Yu, W., et al. (2018). Flow interference between hydraulic fractures. *SPE Reservoir Evaluation & Engineering*, 21(04):942–960.

Westergaard, H. M. (1939). Bearing pressures and cracks: Bearing pressures through a slightly waved surface or through a nearly flat part of a cylinder, and related problems of cracks. *Journal of Applied Mechanics*, 6(2):A49–A53.

Yan, C. and Zheng, H. (2017). Fdem-flow3d: A 3d hydro-mechanical coupled model considering the pore seepage of rock matrix for simulating three-dimensional hydraulic fracturing. *Computers and Geotechnics*, 81:212–228.

Yu, L.-Y., Jing, H.-W., and Wang, Y.-C. (2014). Elastic analysis for subaqueous tunnel surrounding rock via the complex variable method. *Mathematical Problems in Engineering*, 2014:1–6.

Zaadnoordijk, W. J. (1990). *Analytic elements for transient groundwater flow*. PhD thesis, University of Minnesota.

Zaadnoordijk, W. J. and Strack, O. D. L. (1993). Area sinks in the analytic element method for transient groundwater flow. *Water Resources Research*, 29(12):4121–4129.

Zeng, G.-s., Cai, H., and Lu, A.-z. (2019). An analytical solution for an arbitrary cavity in an elastic half-plane. *Rock Mechanics and Rock Engineering*, 52(11):4509–4526.

Zhang, X. and Sanderson, D. J. (1996). Effects of stress on the two-dimensional permeability tensor of natural fracture networks. *Geophysical Journal International*, 125(3):912–924.
Zhao, Y., Liu, Q., Zhang, C., Liao, J., Lin, H., and Wang, Y. (2021). Coupled seepage-damage effect in fractured rock masses: Model development and a case study. *International Journal of Rock Mechanics and Mining Sciences*, 144:104822.
Zimmerman, R. W. (1990). *Compressibility of sandstones*. Elsevier.
Zimmerman, R. W. and Bodvarsson, G. (1995). Effective transmissivity of two-dimensional fracture networks. Technical report, Lawrence Berkeley National Laboratory. LBNL Report: LBL-37332.
Zimmerman, R. W. and Bodvarsson, G. S. (1996). Hydraulic conductivity of rock fractures. *Transport in porous media*, 23:1–30.

Acta Universitatis Upsaliensis

Digital Comprehensive Summaries of Uppsala Dissertations from the Faculty of Science and Technology 2311

Editor: The Dean of the Faculty of Science and Technology

A doctoral dissertation from the Faculty of Science and Technology, Uppsala University, is usually a summary of a number of papers. A few copies of the complete dissertation are kept at major Swedish research libraries, while the summary alone is distributed internationally through the series Digital Comprehensive Summaries of Uppsala Dissertations from the Faculty of Science and Technology. (Prior to January, 2005, the series was published under the title "Comprehensive Summaries of Uppsala Dissertations from the Faculty of Science and Technology".)

Distribution: publications.uu.se
urn:nbn:se:uu:diva-511929

ACTA UNIVERSITATIS
UPSALIENSIS
2023